Science Bulletin 64 (2019) 730–747

Contents lists available at ScienceDirect

Science Bulletin

journal homepage: www.elsevier.com/locate/scib

Science Bulletin
www.scibull.com

Article

Miro2 supplies a platform for Parkin translocation to damaged mitochondria

Jiu-Qiang Wang [a,d,1], Shu Zhu [a,c,d,1], Yihan Wang [a,d,1], Fengli Wang [a,d,1], Chaoqiang An [a,d,1], Dongfang Jiang [a,d], Lijie Gao [a,d], Yingfeng Tu [a,d], Xuefei Zhu [a,d], Yun Wang [a,d], Hongmei Liu [a,d], Juanjuan Gong [a,d], Zhongshuai Sun [b], Xi Wang [a,d], Leimei Liu [a], Keyan Yang [a,d], Caixia Guo [b,*], Tie-Shan Tang [a,d,*]

[a] State Key Laboratory of Membrane Biology, Institute of Zoology, University of Chinese Academy of Sciences, Chinese Academy of Sciences, Beijing 100101, China
[b] Key Laboratory of Genomics and Precision Medicine, Beijing Institute of Genomics, University of Chinese Academy of Sciences, Chinese Academy of Sciences, Beijing 100101, China
[c] Department of Foresight and Evaluation Research, Chinese Academy of Science and Technology for Development, Beijing 100038, China
[d] Institute for Stem Cell and Regeneration, Chinese Academy of Sciences, Beijing 100101, China

ARTICLE INFO

Article history:
Received 19 April 2019
Received in revised form 21 April 2019
Accepted 22 April 2019
Available online 2 May 2019

Keywords:
Miro2
Parkin
Mitochondria
Ca^{2+}
Mitophagy
PINK1

ABSTRACT

PINK1/Parkin-mediated mitophagy is an important process in selective removal of damaged mitochondria, in which translocation of Parkin to damaged mitochondria is recognized as an initiation step. At present, how the damaged mitochondria are selectively recognized and targeted by Parkin is not fully understood. Here we show that Miro2, an outer mitochondrial membrane protein, undergoes demultimerization from a tetramer to a monomer and alteration in mitochondrial localization upon CCCP treatment, suggesting a CCCP-induced realignment of Miro2. The realignment of Miro2 is tightly regulated by PINK1-mediated phosphorylation at Ser325/Ser430 and by Ca^{2+} binding to EF2 domain, which are both essential for the subsequent Parkin translocation. Interestingly, ablation of Miro2 in mouse causes delayed reticulocyte maturation, lactic acidosis and cardiac disorders. Furthermore, several Miro2 mutations found in the congenital lactic acidosis patients also disable its realignment and Parkin translocation. These findings reveal an important role of Miro2 to mediate Parkin translocation by sensing both depolarization and Ca^{2+} release from damaged mitochondria to ensure the accuracy of mitophagy.

1. Introduction

Parkinson's disease (PD) is the most common movement disorder characterized by the dysfunction and loss of dopaminergic (DA) neurons in the substantia nigra, and is closely linked to mitochondrial dysfunction. *PINK1* (PTEN-induced putative kinase 1) and Parkin are causal genes for autosomal recessive early-onset Parkinsonism and key components for mediating mitochondrial quality control [1–3]. The *PINK1* gene encodes a serine/threonine kinase with a predicted mitochondrial target sequence and a putative transmembrane domain at the N terminus [4]. PINK1 is constitutively proteolysed by the mitochondrial rhomboid protease-PARL at the mitochondrial membrane in healthy mitochondria [5,6]. Loss of the mitochondrial membrane potential leads to the accumulation and activation of PINK1 on the mitochondrial outer membrane [7–9], subsequently phosphorylating downstream signal proteins to initiate mitophagy [10–16]. Parkin, an E3 ligase, is one of the downstream signal proteins of PINK1 [8,17,18]. During the process of mitophagy, Parkin is activated by PINK1 and ubiquitin [11,12,17–19], and then translocates from cytoplasm to damaged mitochondria to ubiquitinate numerous mitochondrial outer membrane proteins [1,20,21]. The recruitment of cytosolic Parkin to the mitochondria is believed to be the first step of mitophagy for the removal of damaged mitochondria. Due to the occurrence of ubiquitin phosphorylation by PINK1 in the vicinity of mitochondrial outer membrane, Parkin should translocate proximal to the mitochondrial outer membrane in order to be activated [11]. Therefore, we reasoned there should be mitochondrial outer membrane proteins supplying the platform for Parkin activation.

* Corresponding authors.
E-mail addresses: guocx@big.ac.cn (C. Guo), tangtsh@ioz.ac.cn (T.-S. Tang).
[1] These authors contributed equally to this work.

https://doi.org/10.1016/j.scib.2019.04.033
2095-9273/

Miro1 (RHOT1) and Miro2 (RHOT2) belong to a mitochondrial subfamily of the Ras GTPases. They are both 618 amino acids in length, and possess 60% amino acid identity [22]. They contain two GTPase domains, which flank two calcium-coordinating EF hand domains [23]. Owing to their EF hand domains, Miros can regulate mitochondrial mobility by sensing Ca^{2+} change [24–27]. In addition, the protein levels of Miros can be downregulated by PINK1 and Parkin [28,29]. Interestingly, distinct from the rapid degradation of Miro1, Miro2 protein level can be maintained for a much longer time, even when both PINK1 and Parkin are overexpressed [28], suggesting that Miro2 may play different roles in mitochondrial health maintenance.

Here we investigated the role of Miro2 in mitophagy. We found that, in response to CCCP treatment, Miro2 undergoes a realignment, which is essential for Parkin recognition and translocation. We then determined that Miro2 is a direct substrate of PINK1, which can immediately phosphorylate Miro2 at Ser325/Ser430 when mitochondrial membrane potential collapses. Intriguingly, both PINK1-mediated phosphorylation of Ser325/Ser430 and Ca^{2+} binding to EF2 domain are essential for the Miro2 realignment and subsequent Parkin translocation to damaged mitochondria, indicating that Miro2 senses both PINK1 activity and Ca^{2+} release from mitochondria to enable that damaged mitochondria to be targeted by Parkin during the initiation of mitophagy. Consistently, the amount of abnormal mitochondria was aberrantly increased in cardiomyocytes derived from Miro2-KO mice. We provide biochemical, molecular cellular, and in vivo mouse model data demonstrating that Miro2 functions as a platform for Parkin-mediated quality control, and the deficiency of which could be a key underlying mechanism for human cardiac disorders.

2. Materials and methods

2.1. Constructs

The following constructs are constructed by our lab and the details on their construction are available upon request: mito-DsRed and mito-GFP; hPINK1-Flag and GST-hPINK1Δ1-140; GFP-hParkin; DsRed-hParkin; Flag-hParkin; pEGFP-C3-hMiro1; pEGFP-C3-hMiro2; pDsred-express-C1-MARCH5; pDsred-express-C1-MUL1; pEYFP-C3-Miro1; pEYFP-C3-Miro2; pEYFP-C3-Miro2 (ΔEF1); pEYFP-C3-Miro2 (ΔEF2); pEYFP-C3-Miro2 (ΔEF2); pEGFP-C3-Exon10; pEGFP-C3-A88T, pEGFP-C3-R245Q, pEGFP-C3-R425C, pEGFP-C3-S325A, pEGFP-C3-S430A, pEGFP-C3-S325/430A, pEGFP-C3-S555A, pEGFP-C3-E208K, pEGFP-C3-E328K, pEGFP-C3-E208/328 K, pEGFP-C3-T18N, pEGFP-C3-S430N, pEGFP-C3-T18N/S430N, pEGFP-C3-A13V, pEGFP-C3-R425V, pEGFP-C3-A13V/R425V, SBP-2*Flag-S325A, SBP-2*Flag-S430A, SBP-2*Flag-S325/ 430A and SBP-2*Flag-S555A were generated by site-directed mutagnesis. pEGFP-C3-hMiro2 (ΔEF1), pEGFP-C3-hMiro2 (ΔEF2), pEGFP-C3-hMiro2 (ΔGTPase1), pEGFP-C3-hMiro2 (ΔGTPase2) were generated by PCR amplification from pEGFP-C3-Miro2 and then ligated into the pEGFP-C3 vector.SBP-2*Flag-hMiro2 (Δ1-143), SBP-2*Flag-hMiro2 (Δ1-183), SBP-2*Flag-hMiro2 (Δ1-219), SBP-2*Flag-hMiro2 (Δ1-303), SBP-2*Flag-hMiro2 (Δ1-339), SBP-2*Flag-hMiro2 (Δ1-410), SBP-2*Flag-hMiro2 (Δ1-530), SBP-2*Flag-hMiro2 (1–303), SBP-2*Flag-hMiro2 (1–339), SBP-2*Flag-hMiro2 (1–410), SBP-2*Flag-hMiro2 (1–531), SBP-2*Flag-hMiro2 (1–570) and SBP-2*Flag-hMiro2 (Δ301-410), SBP-2*Flag-hMiro2 (Δ301-580) were generated by PCR amplification from pEGFP-C3-Miro2 and then ligated into SBP-2*Flag vector. SBP-2*Flag-hMiro1 (Δ301-410) was generated by PCR amplification from pEGFP-C3-Miro1 and then ligated into SBP-2*Flag vector.

2.2. Cell culture, transfection and CCCP treatment

Mouse embryonic fibroblast cells (MEFs) and 293 T cells were maintained at 37 °C with 5% CO_2 atmosphere in DMEM (Invitrogen) supplemented with 10% FCS. Authentication testing of HEK 293 T cell lines have been performed by Shanghai Biowing Applied Biotechnology Co., Ltd via STR profiling. STR profiles match the standards recommended for HEK 293 T cell lines authentication. Plasmids were transfected with polyethylenimine (PEI, 1 mg/mL) as previous report [30]. Collapse of mitochondrial membrane potential was achieved with 20 μmol/L carbonyl cyanide m-chlorophenylhydrazone (CCCP, Sigma) at the indicated times.

2.3. RNA interference

To knock down mouse Miro1 and Miro2, siRNAs against Miro1 and Miro2 were synthetized as the following sequences: GCTCAACTTCTTCCAGAGAAT for Miro1-1; GATGATCATAAGTCCTATTAT for Miro1-2, TACCATATACAAGCGTTATTA for Miro2-1; TTCGGCCTGTTGGAGTAATAT for Miro2-2, respectively. A scrambled siRNA was used as control and was synthesized as the following sequence: TTCTCCGAACGTGTCACGT. mPINK1 silencing was used as the following sequence: CCTGGCTGACTATCCTGATAT. MEFs were transfected with 10 nmol/L siRNA on three consecutive days using Lipofectamine RNAiMAX (Invitrogen) according to manufacturer's instruction. Silenced cells were transferred to 3.5 cm confocal dishes, transfected with corresponding plasmids the next day and then treated with 20 μmol/L CCCP for 6 h. After CCCP treatment, cells were washed with PBS, fixed with 4% paraformaldehyde (PFA) for 10 min at room temperature and then maintained with PBS.

2.4. Chemicals and antibodies

The following chemicals were used in this study: Rhosin (Tocris Bioscience, 5003); Cyclosporin A (Abcam, ab120114); CPG37157 (Sigma, C8874); Bongkrekic acid (Millipore, 203671); disuccinimidyl suberate (DSS, Thermo); tetramethylrhodamine methyl ester (TMRM, Thermo).

The following antibodies were used in this study: anti-GFP (Santa Cruz, SC-8334); anti-phospho-serine (Ruiyingbio, RLM3440); anti-Miro1 (Santa Cruz, sc-292547); anti-Miro2 (Abcam, ab154946); anti-Flag antibody (Sigma, F7425); anti-actin (Proteintech, 60008-1); anti-PINK1 (Novus, BC100-94); anti-TIM23(BD, 611223); anti-COXIV (CST, 4844); anti-GAPDH (Proteintech, 60004-1); anti-cyto D (Abcam, ab110324); anti-MCU (Sigma, HPA016480); anti HA beads (Sigma, E6779); anti Flag M2 beads (Sigma, A2220).

2.5. Immunoprecipitation and immunoblotting

293 T cells were washed with PBS and lysed in NETN lysis buffer (100 mmol/L NaCl, 1 mmol/L EDTA, 20 mmol/L Tris-HCl, pH 8.0, 0.5% NP-40) containing protease inhibitor (AMRESCO) for 30 min at 4 °C. Cell debris was pelleted at 17,000 *g* for 10 min and the cell supernatant was collected. For Immunoprecipitation, the cell supernatant was incubated with anti-Flag M2 beads for 3 h at 4 °C and then centrifuged at 7,000 *g* for 1 min to collect anti-Flag

M2 beads. The collected M2 beads was washed three times with lysis buffer and then boiled with loading buffer at 100 °C.

MEFs were lysed in 200 μL loading buffer, boiled for 10 min at 100 °C and pelleted at 1,7000 *g* for 10 min. Samples were separated on 10% polyacrylamide gels and transferred to PVDF membranes. Membranes were blocked in 10% milk in TBS-T, incubated overnight with primary antibody at 4 °C, followed by incubation with HRP-conjugated secondary antibodies for 2 h at room temperature. Membranes were visualized using Immobilon Western chemiluminescent HRP substrate (Millipore) on image quant LAS 4000 (GE).

2.6. Cell imaging

Live cell images were acquired using confocal laser scanning microscope and 3D structured illumination microscopy (NiKon N-SIM). The cultured MEFs on 3.5 cm confocal dishes were changed to L-15 medium (sigma, L1518) supplemented with 10% FCS before images were acquired. After treatment with 20 μmol/L CCCP for 0.5 h, cells were imaged within 1 h after CCCP treatment. During image acquisition, cells were always cultured at L-15 medium containing CCCP. Images were acquired first using confocal laser scanning microscope to obtain the full view images and then secondarily acquired using N-SIM. All images were acquired with N-SIM and then reconstructed using NIS-Elements software (Nikon Instruments, Melville, NY).

To image the mitochondrial membrane potential, YFP-Miro2 and GFP-Parkin co-overexpressed MEFs were stained with 20 nmol/L TMRM at 37 °C for 20 min, and then imaged using a Leica DMI6000B total internal reflection fluorescence microscope (Leica). 20 μmol/L CCCP was used to destroy mitochondrial membrane potential for 6 h. TMRM intensity is measured with Image J. To calculate the relative TMRM intensity, the TMRM fluorescence intensity of each group is normalized to that of GFP-hParkin and mito-YFP co-expressing group.

MEFs were treated with 20 μmol/L CCCP for 6 h and then fixed with 4% paraformaldehyde (PFA). The fixed cells were maintained in PBS and were imaged using a Leica DMI6000B total internal reflection fluorescence microscope (Leica). Due to the difficulty in distinguishing the positive knocked down cells, the images were randomly acquired more than 100 fields and only the GFP and Dsred double positive cells were recognized as target cells in each experiment. Co-localization of Parkin and mitochondria was assessed by visually scoring $\geq$150 Parkin positive cells per condition in each experiment. For quantification of Parkin translocation, only complete overlap of Parkin and mitochondria was considered as positive.

Fluorescence of mt-Keima was imaged in 2 channels via 2 sequential excitations (458 nm, green; 561 nm, red) and using a 609- to 735-nm emission range as described in a previous report [31]. For quantitative analysis of mitophagy with mt-keima, the ratio of the area of lysosomal (red) signal to mitochondrial (green) signal can be used as a measure of lysosomal delivery of mitochondria.

2.7. In vivo and in vitro kinase assay

For the in vivo kinase assay, wild-type or mutants of Miro2 bearing with SBP and flag tags were overexpressed in 293 T cells and then treated with DMSO or CCCP for 30 min. After treatment with CCCP, cells were lysed with 1 mL 1x SDS loading buffer and boiled for 10 min at 100 °C. The lysates was then diluted with 9 mL NETN lysis buffer and incubated with anti-Flag M2 beads at 4 °C overnight. M2 beads were collected by centrifugation at 7,000 *g* and washed with NETN lysis buffer 3 times. The purified protein bearing M2 beads was boiled with 1X SDS loading buffer at 100 °C and then separated on a 10% polyacrylamide gel. After the gel was transferred to a PVDF membrane, the membrane was blocked with 10% milk in TBS-T, incubated overnight with anti-phosphoserine antibody at 4 °C, followed by incubation with HRP-conjugated secondary antibodies for 2 h at room temperature. Membranes were visualized using Immobilon Western chemiluminescent HRP subatrate (Millipore) on an image quant LAS 4000 (GE).

For in vitro kinase assays, wild-type and mutants of Miro2 bearing with SBP and flag tags were overexpressed in 293 T cells and then purified via their flag tags by immunoprecipitation. Then the flag beads bearing either wild-type or mutants Miro2 were incubated with GST-hPINK1 1-140 in PINK1 kinase reaction buffer, respectively. Reactions were set up in a volume of 25 μL, using 2 μg of wild-type or mutants of Miro2 and 1 μg of *E. coli*-expressed GST-hPINK1Δ1-140, in 50 mmol/L Tris/HCl (pH 7.5), 0.1 mmol/L EGTA, 10 mmol/L $MgCl_2$, 2 mmol/L DTT, 120 mmol/L KCl, 0.1% Trioton-X 100 and 10 μci [γ-32P] ATP. Assays were incubated at 30 °C for 60 min and then terminated with 2 mmol/L pre-cooled ATP. Flag beads were collected by centrifugation at 7,000 g and then boiled with 1 × SDS loading buffer at 100 °C. After separation on a 10% polyacrylamide gel, gels were wrapped with plastic wrap and then covered with phosphor screen for overnight. Incorporation of [γ-32P] ATP into substrates was analyzed by imaging with a Phosphor screen on a FLA-7000 (Fujifilm). To quantify the concentration of GST-hPINK1Δ1-140 in different samples, the gel was transferred to a PVDF membrane and the memebrane was stained with Ponceau Red.

2.8. Phos-tag™ SDS-PAGE

Mobility shift detection of phosphorylated proteins by using Phos-tag™ SDS-PAGE was performed according to the manufacturer's protocol (Wako, Japan). Briefly, 20 μg total protein was size-separated on 8% polyacrylamide gels containing 20 μmol/L phos-tag acrylamide and 100 μmol/L $MnCl_2$. Gels were washed with transfer buffer containing 1 mmol/L EDTA for 10 min at room temperature and then with transfer buffer without EDTA for another 10 min. Proteins were transferred to PVDF membranes and immunoblotting performed using chemiluminescence detection on X-ray film.

2.9. Chemical cross-linking and mass spectrometry

Chemical cross-linking was accomplished according to the manufacturer's protocol. Briefly, Cultured 293 T cells expressing GFP-Miro1 or GFP-Miro2 were treated with 20 μmol/L CCCP at the indicated time, collected and rinsed twice with ice-cold PBS. Then, the cross-linking reagent dsuccinimidyl suberate (DSS, Thermo) was added to the rinsed cells to a final concentration of 0.5 mmol/L and incubated with for 40 min at RT. The reaction was stopped by the addition of Tris-HCl (1 mol/L, pH 8.0) to a final concentration of 100 mmol/L for 15 min at RT. The quenched samples were subsequently mixed with 5 × concentrated SDS loading buffer containing 50 mmol/L DTT, incubated at 75 °C for 10 min, and then subjected to electrophoresis.

Miro1 or Miro2 bearing a flag tag was overexpressed in 293 T cells, and then cross-linked with DSS to a final concentration of 0.5 mmol/L. After stopping the cross-linking reaction by the addition of Tris-HCl, the collected cells were lysed with 1 mL of 1 × SDS loading buffer and boiled at 100 °C for 5 min. The lysis solution was

then diluted with 9 mL NETN lysis buffer and incubated with anti-Flag M2 beads at 4 °C for whole night. M2 beads were collected by centrifugation at 7,000 *g* and washed with NETN lysis buffer 3 times. The bound proteins were eluted by boiling in SDS sample buffer, resolved by SDS-PAGE and visualized by silver staining. Bands at ~310 kD on the gel was cut out and digested for mass spectrum analysis.

2.10. Transmission electron microscopy

MEFs and RBCs were fixed with 2.5% glutaraldehyde and embedded in Spurr's low viscosity resin similar to described protocols [32]. After staining with uranyl acetate and lead citrate, Sections were analysed using a Tecnai F20 TWIN TMP transmission electron microscope (FEI, Netherlands).

Ultrastructural examination of osmium tetroxide/uranyl acetate stained mouse heart sections (90 nm) used a Jeol electron microscope (JEM-1400) (JEOL, Japan). To compare the number of abnormal mitochondria in cardiomyocytes, the diameter of mitochondria greater than 1 μm was deemed to be abnormal mitochondria.

2.11. Glycolysis stress test

Glycolysis stress tests were performed for WT and Miro2 KO MEFs using the Seahorse Extracellular Flux (XF-96) analyzer. Cells were cultured for 2 h in the absence of glucose. *D*-glucose (30 mmol/L), oligomycin (2 μmol/L), and 2-Deoxyglucose (50 mmol/L) were sequentially injected into the cell culture Microplates. Glycolysis was defined as ECAR following the addition of *D*-glucose and maximum glycolytic capacity was defined as ECAR following the addition oligomycin. ECAR following treatment with 2-Deoxyglucose is associated with non-glycolytic activity.

2.12. Hematoxylin and eosin (HE) staining

Histological studies were performed on mouse hearts fixed with 4% formaldehyde solution in PBS. Tissues were paraffin-embedded and sectioned at a thickness of 5 μm on a Leica RM2255 rotary microtome. The sections were de-paraffinized in xylene and rehydrated with a gradient (100%–50%) of ethanol, followed by a wash in distilled water. Sections were stained with hematoxylin and eosin (H&E) and then examined with PerkinElmer Vectra Slide Analysis System (PerkinElmer). To obtain statistics on the mean cell thickness of myocardial fiber in indicated sections, we choose the shortest distance between nucleus and cell membrane.

2.13. Mice

Miro2 knockout C57 BL/6J mice were generated by deleting the region spanning from the second to the forth exons of Miro2 in zygotes using the CRISPR/Cas9 system by CasGene Biotechnology Company limited (Beijing, China). The sequences of gRNA used in this mouse model generation were ccgcgggaagaccggtagggtcg and cctggcggctggattaggtgact. *D*-lactic acid ELISA assay (Qingdao Jiskang Biotech, China) was performed according to manufacturer's instruction. All animal experiments were reviewed and approved by the Institute of Zoology Institutional Animal Care and Use Committee and were conducted according to the committee's guidelines.

2.14. Statistical analysis

We used *t*-test analysis to compare paired comparisons and one-way ANOVA along with Bonferroni correction to compare multiple comparisons. Data are expressed as the mean ± SEM of at least three independent experiments, and $P < 0.05$ were considered statistically significant.

3. Results

3.1. Miro2 facilitates Parkin translocation to depolarized mitochondria

PINK1 and Parkin regulate mitochondrial mobility by changing the protein levels of Miro1 and Miro2 [28]. Interestingly, Miro1 and Miro2 manifest distinct degradation rates in response to CCCP treatment [28]. Considering Miro2 is more stable than Miro1, we speculated that Miro2 might play additional roles in mitophagy beyond influencing mitochondria mobility. To test this hypothesis, we overexpressed Miros in MEFs and then imaged with both Confocal and structured illumination microscopy N-SIM, a form of super-resolution microscopy with an axial resolution of about 100 nm. Under unperturbed conditions, Miro1 and Miro2 completely overlapped with mitochondrial marker mito-DsRed (Fig. 1a, b). In response to CCCP treatment for <1 h, Miro1 still co-localized with mitochondria (Fig. 1a). However, Miro2 clearly formed a thin layer surrounding mito-DsRed under N-SIM super resolution microscopy (Fig. 1b). We then co-expressed Miro2 with MARCH5 or MUL1 in MEFs to test whether the change in mitochondrial distribution also applied to other mitochondrial outer membrane proteins. MARCH5 and MUL1 (MAPL) primarily localize on mitochondrial outer membrane [33,34]. In response to CCCP treatment, Miro2 again underwent the change in mitochondrial distribution (Fig. S1a, b online). However, analogous to Miro1, MARCH5 and MUL1 showed no alteration in mitochondrial distribution before and after CCCP treatment (Fig. S1a, b online). Interestingly, although Miro2 has sustained the change in distribution, it still completely overlapped with the MARCH5 and MUL1, indicating that CCCP treatment did not alter the co-localization of Miro2 with mitochondria.

Given that Miro2 is an outer mitochondrial transmembrane protein, we believed that Miro2 could be realigned or organized in response to CCCP assault. Therefore, we used protein cross-linker reagent DSS to test whether CCCP treatment affects the formation of Miros polymers in living cells. In contrast to previous reports [35,36], we found that both Miro1 and Miro2 form a putative tetramers (~310 kD) rather than dimers under unperturbed conditions (Fig. S1c, d online). Upon CCCP treatment, Miro2 tetramers demultimerized to monomer, whereas Miro1 tetramers remained intact (Fig. S1c, d online). Moreover, we found that a Miro2 truncation (Δ1-303), which can prevent its self-interaction, abolished the formation of Miro2 tetramer (Fig. S1e, f online). Klosowiak et al. [35] report that the C-terminal GTPase (cGTPase) domain of hMiro forms an interface with the second hidden EF hand (hEF2). However, deletion of GTPase2 and EF hand domains of Miro2 (Δ303-580) showed little effect on its self-interaction and the tetramer formation (Fig. S1g, h online). These results support that Miro2 forms tetramers rather than dimers in living cells. To explore the nature of the complex of 310 kD, we analyzed the components of each Miros complex with mass spectrometry (Fig. S1 online). The results showed that the components of the complex of 310 kD are primarily either Miro1 or Miro2 respectively, suggesting that the ~310 kD Miro2 (or Miro1) complex is a homo-tetramer of Miro2 (or Miro1) (Fig. S1j, k online). These data collectively indicate that the CCCP-

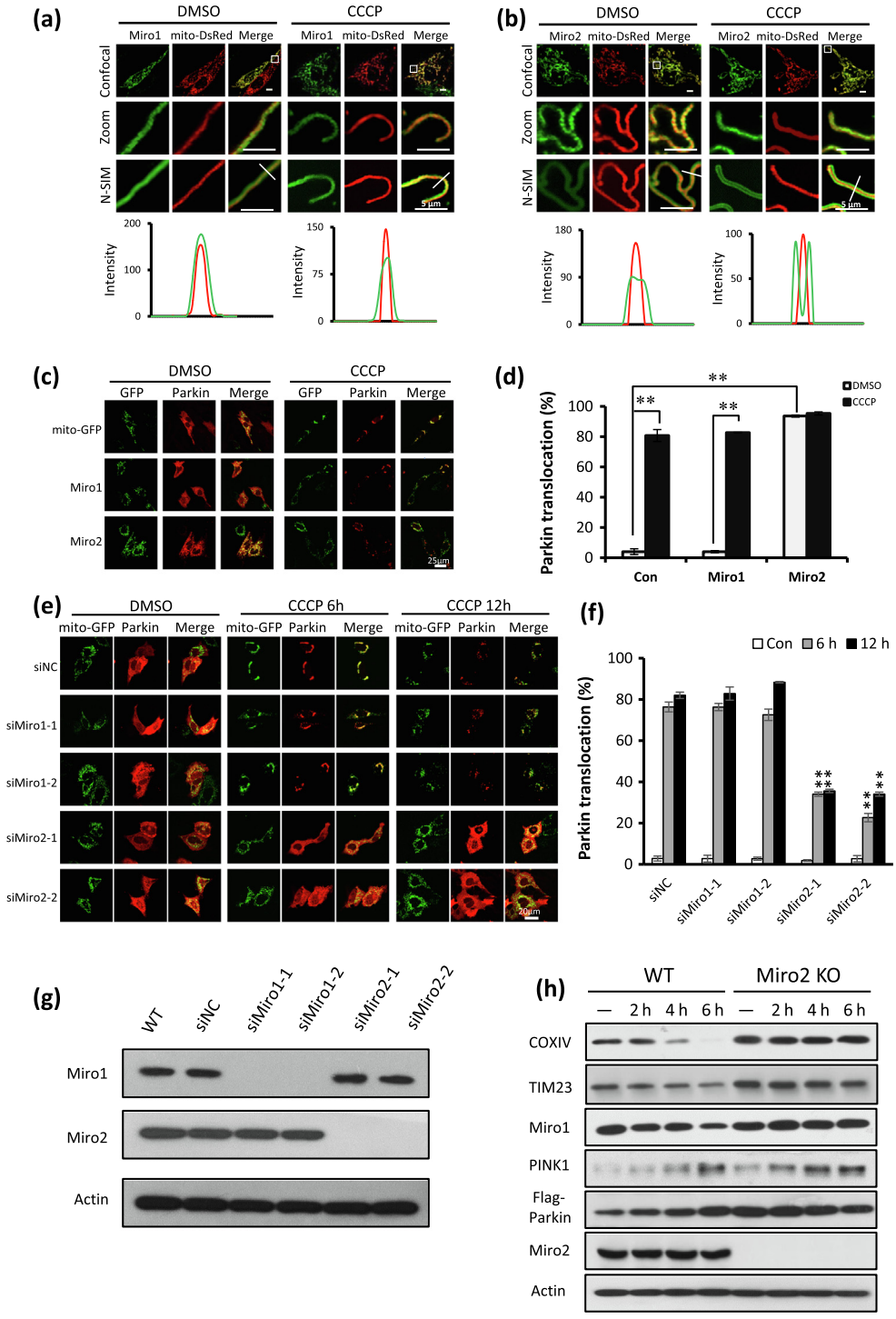

Fig. 1. Miro2 facilitates Parkin translocation to depolarized mitochondria. (a) Representative N-SIM images showing the co-localization of GFP-Miro1 with mito-DsRed. MEFs co-expressing GFP-Miro1 and mito-DsRed were imaged within 1 h of treatment with DMSO or 20 μmol/L of CCCP. Images were first acquired by confocal microscopy and then with N-SIM. Note that since the images were acquired on living cells, the images from different fluorescence channels may have shifted slightly due to active mitochondrial mobility during confocal and N-SIM image capture. The first row shows the image acquired by confocal microscopy, the second row shows the enlarged image of the confocal image, the third row shows the image acquired with N-SIM microscopy. The forth row shows the fluorescence intensity profiles of Miro1 (*green*) and mito-DsRed (*red*) across mitochondria. The fluorescence intensity profiles were taken across the area indicated by a white line in N-SIM images. (b) Representative N-SIM images showing the realignment of Miro2 in response to CCCP treatment. MEFs co-expressing GFP-Miro2 and mito-DsRed were treated and imaged as in (a). N-SIM fluorescence intensity profile of Miro2 (*green*) and mito-DsRed (*red*) shows a change in the mitochondrial distribution of Miro2 in response to CCCP treatment. (c, d) Miro2 overexpression significantly promotes Parkin translocation. MEFs co-expressing DsRed-Parkin with mito-GFP, GFP-Miro1 or GFP-Miro2 were treated with 20 μmol/L of CCCP for 6 h and then fixed with 4% PFA. Complete overlap of DsRed-Parkin with GFP is considered to represent Parkin translocation, and this applies for all Parkin translocation assays. (e–g) Knock-down of Miro2 significantly reduces Parkin translocation. Transient Miro1 or Miro2 knock-down MEFs were co-transfected with DsRed-Parkin and mito-GFP. MEFs were treated with 20 μmol/L of CCCP for the indicated time and then fixed with 4% PFA. siNC stands for the non-specific siRNA (negative control), and this applies to all other figures. (h) Miro2 deficiency inhibits mitochondrial proteins degradation. WT and Miro2-KO MEFs overexpressing Flag-Parkin were treated with DMSO or 20 μmol/L of CCCP for the indicated time. $^{**}P < 0.01$. Data are from three independent experiments and the results are presented as mean ± SEM.

induced change in Miro2 mitochondrial distribution represents a demultimerization from tetramer to monomer, which we referred to as realignment thereafter.

We next wanted to know whether Miro1 and/or Miro2 play a role in mitochondrial damage-induced Parkin translocation. Under unperturbed conditions, Miro1 overexpression did not alter the distribution of Parkin (Fig. 1c, d). Surprisingly, Miro2 overexpression significantly promoted Parkin translocation to mitochondria even without CCCP exposure (Fig. 1c, d). In response to CCCP treatment, Parkin translocation was significantly elevated in Miro1-overexpressed cells; while in Miro2-overexpressed cells, CCCP treatment did not cause a further increase in Parkin translocation compared with the untreated group (Fig. 1c and d). In addition, Parkin also formed a thin layer surrounding Miro2 in Miro2/Parkin co-expressed cells before and after CCCP treatment (Fig. S1g online). Since co-expression of Miro2 and Parkin resulted in a decrease of mitochondrial membrane potential in MEFs even without CCCP treatment (Fig. S2a, b online), we conclude that the Parkin translocation induced by co-expression of Miro2 and Parkin was also PINK1 activity-dependent.

To further examine the role of Miro2 in Parkin translocation, we knocked down Miro1 and Miro2 with siRNA. We found that knocking-down Miro1 or Miro2 did not alter the morphology of mitochondria and the distribution of Parkin in the unperturbed condition (Fig. 1e–g). In response to CCCP treatment, however, silencing of Miro2 significantly decreased Parkin translocation compared with the siRNA controls (Fig. 1e–g), whereas knocking-down Miro1 had no effect on CCCP-induced Parkin translocation (Fig. 1e–g). Moreover, Miro2 deficiency obviously inhibited CCCP-induced degradation of mitochondrial proteins (Fig. 1h, Fig. S2c online) and the clearance of mitochondrial mass (Fig. S2e, f online). Importantly, Miro2 loss significantly blocked mitophagy (Fig. S2g, h online). Notably, loss of both Miros obviously promoted the degradation of mitochondrial proteins (Fig. S2d online) which was consistent with the previous report [28]. Based on above results, we conclude that Miro2, but not Miro1, undergoes a realignment and promotes Parkin translocation to depolarized mitochondria during the initiation of mitophagy.

3.2. Miro2 dynamically interacts with PINK1 and is phosphorylated by PINK1

Our data show that Miro2 deficiency blocks Parkin translocation, suggesting that Miro2 may act downstream of PINK1. To explore the potentially functional coordination between PINK1 and Miro2 during mitophagy, we first examined the molecular interaction between PINK1 and Miro2 through co-immunoprecipitation. The association between Miro1 and PINK1 was weak under unperturbed conditions, which barely changed in response to CCCP treatment (Fig. 2a, c). However, CCCP treatment markedly enhanced the interaction between Miro2 and PINK1 at 0.5 and 1 h (Fig. 2b, c), indicating a dynamic association between Miro2 and PINK1 during the incipient stage of mitophagy. To map the sequences of Miro2 required for its interaction with PINK1, we constructed a series of Miro2 truncations. By deleting sequences from the N-terminus and C-terminus, we found that the sequences spanning from 339 to 410 of Miro2 were important for its interaction with PINK1 (Fig. S3a–d online). Since the sequences from 1 to 339 exhibited a partial interaction with PINK1 (Fig. S3d online), we then constructed a Δ301-410 deletion to check its interaction with PINK1. We found that deletion of aa 301–410 in Miro2 nearly abolished Miro2 interaction with PINK1 (Fig. S3e online), suggesting that aa 301–410 contains the critical regions mediating Miro2 association with PINK1. Furthermore, we also compared the interaction of Parkin with Miro1 and Miro2. Our results showed that there was a strong interaction between Miro2 and Parkin (Fig. S3f online). Surprisingly, we detected no visible interaction between Miro1 with Parkin under unperturbed conditions (Fig. S3f online). Therefore, differences in the interaction of Miros with PINK1 and Parkin likely account for the isoform-specific role of Miro2 in Parkin recruitment during mitophagy.

Since Miro2 dynamically interacts with PINK1 in response to CCCP treatment, we next sought to determine if Miro2 could be phosphorylated by PINK1. We first determined whether Miro2 undergoes phosphorylation using phosphorylated-protein-affinity SDS-PAGE (Phos-tag™ SDS-PAGE), in which, the small molecule Phos-tag binds to acrylamide and two Mn^{2+} ions, such that phosphorylated proteins are captured by the Mn^{2+}-Phos-tag and migrate more slowly than non-phosphorylated proteins. Phos-tag™ SDS-PAGE analysis showed that Miro2 was quickly phosphorylated at 0.5 and 1 h after CCCP-treatment (Fig. 2d). Under the same condition, Miro1 manifested no phosphorylation (Fig. 2d). Then, we used ^{32}P-labelled in vitro kinase assays to determine whether PINK1 can phosphorylate Miro2. Bacterially-expressed GST-tagged PINK1 Δ1-140 was purified and incubated with purified Miro2 bearing SBP and Flag tags in a PINK1 kinase reaction buffer. The results clearly showed that Miro2 was phosphorylated by PINK1 (Fig. 2e). To probe the exact phosphorylation sites in Miro2, we compared the sequences of different species and found that the serines at aa 325, 430 and 555 are all evolutionarily conserved. We next mutated these sites to alanine and evaluated their effects on Miro2 phosphorylation by PINK1 in in vitro kinase assays. We found that, the mutation of serine 325 and/or serine 430 to alanine (S325A, S430A and S325/430A) abolished Miro2 phosphorylation, whereas the mutation at serine 555 (S555A) failed to do so (Fig. 2e), indicating that S325 and S430 are the main phosphorylation sites in Miro2. To further determine the phosphorylation status of these two sites in vivo, we expressed Miro2 and its mutations in 293 T cells and purified by denatured immunoprecipitation to probe their phosphorylation with anti-phosphorylated serine antibody. The results showed that Miro2 was clearly ser-phosphorylated at 0.5 and 1 h after CCCP treatment (Fig. 2f, h). Moreover, the Ser-phosphorylation levels at 0.5 and 1 h were similar after CCCP treatment and then decreased (Fig. 2f, h), indicating a dynamic change of Miro2 phosphorylation at the early stage of mitochondrial damage. Consistently, the above Miro2 serine mutations (S325A, S430A and S325/430A) abolished the dynamic change in phosphorylation upon CCCP treatment (Fig. 2f, h). Additionally, knocking down PINK1 clearly attenuated the CCCP-induced dynamic phosphorylation of Miro2 (Fig. 2i), indicating that the two conserved sites (Ser325 and Ser430) of Miro2 are endogenous PINK1 phosphorylation sites.

Ubiquitin was reported to be phosphorylated during mitophagy [11,12,19]. To validate our experimental system, we also assessed the change of ubiquitin phosphorylation status. Consistent with prior studies [11,12,19], the phosphorylation level of ubiquitin was elevated over the duration of CCCP treatment (Fig. S3h online).

3.3. The PINK1-dependent phosphorylation of Miro2 regulates its realignment and subsequent Parkin translocation

To determine the role of PINK1 in CCCP-induced Miro2 realignment, we selectively knocked down PINK1 in MEFs. We found that Miro2 failed to show a realignment in PINK1-KD MEFs upon CCCP treatment, indicating that the CCCP-induced realignment of Miro2 is PINK1-dependent (Fig. 2j, k). Furthermore, the S325A mutation that disabled the PINK1-mediated Miro2 phos-

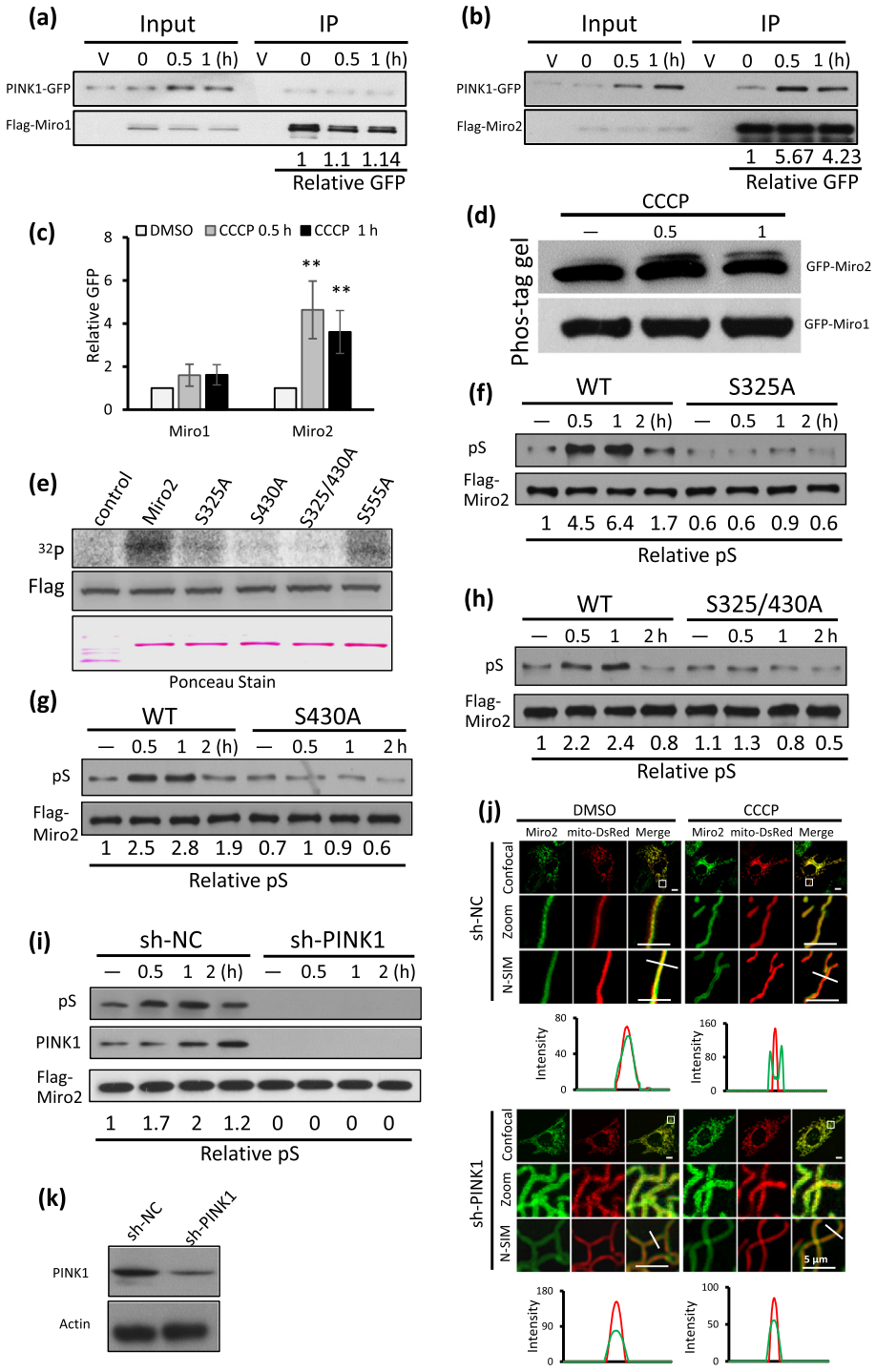

Fig. 2. Miro2 is phosphorylated by PINK1. (a–c) CCCP treatment enhances the interaction of Miro2 with PINK1. The cell lysates from 293 T cells co-expressed PINK1-GFP with Flag-Miro1 (a) or Flag-Miro2 (b) were subjected to immunoprecipitated with anti-Flag M2 beads. In response to CCCP treatment, the interaction of PINK1 and Miro2 was significantly enhanced ($n = 3$), whereas the interaction of PINK1 with Miro1 shows little change ($n = 2$) (c). $^{**}P < 0.01$. The results are presented as mean ± SEM. (d) Miro2 electrophoretic mobility shifts in Phos-Tag™ SDS-PAGE gels. MEFs were overexpressed with GFP-tagged Miro1 or Miro2 and then treated with 20 μmol/L CCCP for the indicated time. (e) Miro2 is phosphorylated by PINK1 in in vitro kinase experiments. PINK1 Δ1-140 bearing a GST tag was expressed in bacteria and purified with GST beads. The purified PINK1 Δ1-140 protein was then incubated with purified Flag-Miro2 or a Flag-Miro2 mutant in PINK1 kinase reaction buffer at 30 °C for 90 min. (f–h) Miro2 is phosphorylated by PINK1 in in vivo kinase experiments. Flag-Miro2 or Flag-Miro2-S325A, Flag-Miro2-S430A or Miro2-S325/430A was expressed in 293 T cells and then treated with 20 μmol/L of CCCP for the indicated time on the next day. Miro2 and its mutations were purified with anti-Flag M2 beads from the cell lysates by denatured immunoprecipitation and blotted with anti-phosph-Ser antibody. (i) PINK1 deficiency attenuates the dynamic phosphorylation of Miro2 in response to CCCP. Flag-Miro2 was expressed in PINK1 knocking down HepG2 cells and then treated with 20 μmol/L of CCCP for the indicated time on the next day. Miro2 was purified with anti-Flag M2 beads from the cell lysates solution by denatured immunoprecipitation and blotted with anti-phospho-Ser antibody. sh-NC stands for the non-specific shRNA (negative control), and this applies to all other figures. (j and k) Knocking-down of PINK1 abolishes the realignment of Miro2 in response to CCCP treatment. Transient PINK1 knock-down MEFs were co-transfected with GFP-Miro2 and mito-DsRed, and then imaged by confocal microscopy and N-SIM as in Fig. 1a. Note that since the images were acquired from the living cells, the images from different fluorescence channels may have shifted due to active mitochondrial mobility during confocal and N-SIM image capture. The fluorescence intensity profiles (Miro2, *green*; mitochondria, *red*) were taken across the area indicated by the white line in N-SIM images.

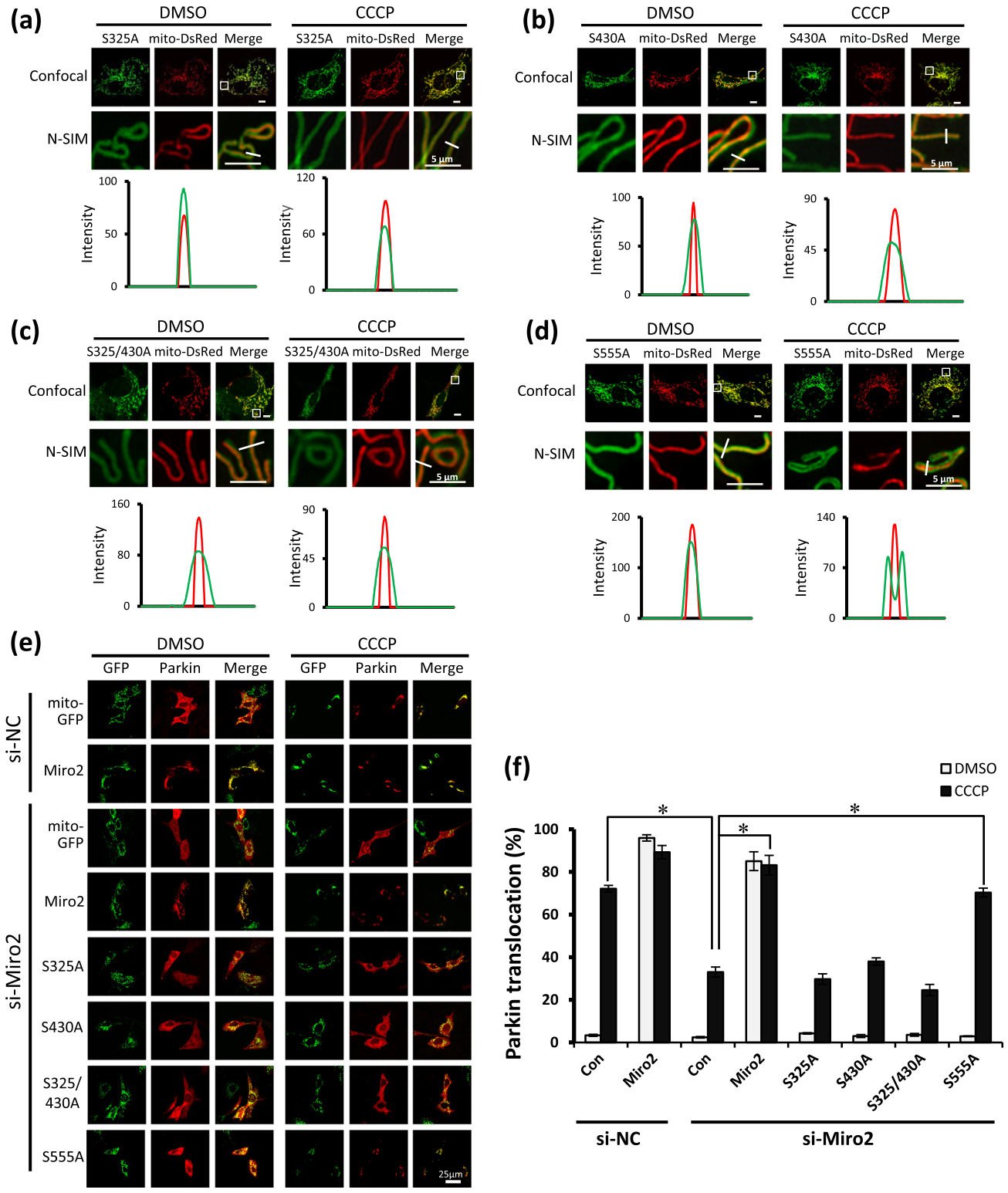

Fig. 3. The phosphorylation of Miro2 by PINK1 recruits Parkin translocation. (a–d) The point mutations at serine 325 and 430 abolish the realignment of Miro2 in response to CCCP treatment. MEFs co-expressing mito-DsRed and GFP-Miro2-S325A, GFP-Miro2-S430A, GFP-Miro2-S325/430A or GFP-Miro2-S555A were treated with 20 μmol/L CCCP and then imaged within 1 h. Note that the fluorescence images from different channels may have shifted due to our having performed confocal and N-SIM imaging on living cells, in which the mitochondria are very mobile. The fluorescence intensity profiles were taken across the area indicated by the white line in N-SIM images. (e and f) Serine 325 and 430 mutants fail to complement Parkin translocation in response to CCCP treatment. Miro2 knocked-down MEFs were co-expressed with DsRed-Parkin and mito-GFP, GFP-Miro2, GFP-Miro2-S325A, GFP-Miro2-S430A, GFP-Miro2-S325/430A or GFP-Miro2-S555A, and then treated with 20 μmol/L CCCP for 6 h. Complete overlap of DsRed-Parkin with GFP was considered to represent Parkin translocation. Miro2 coding sequence has been changed (without changing amino acid sequence) and thus resistant to siRNA against Miro2. $^{*}P < 0.05$. Data are from three independent experiments and the results are presented as mean ± SEM.

phorylation also abolished the CCCP-induced demultimerization of Miro2 tetramers (Fig. S3g online), demonstrating that demultimerization of Miro2 is tightly regulated by PINK1-mediated phosphorylation. To further ascertain the roles of PINK1-dependent Miro2 phosphorylation in mitophagy, we then determined whether mutation of the two conserved serines (S325/S430) influences Miro2 localization change. Under unperturbed conditions, S325A, S430A, S325/430A and S555A all overlapped with mito-DsRed (Fig. 3a–d). Upon CCCP treatment, mutations S325A, S430A and S325/430A but not S555A abrogated this relocalization (Fig. 3a–d), indicating that the realignment of Miro2 leading to relocalization is critically dependent on the phosphorylation at S325/S430. To further establish the direct link between Miro2 phosphorylation status and Parkin translocation, we knocked down Miro2 and performed rescue experiments with wild type Miro2 or mutations respectively (Fig. 3e, f). Knocking-down Miro2 significantly reduced Parkin translocation in response to CCCP treatment (Fig. 3e, f), which could be completely rescued by re-expression of wild type Miro2 (Fig. 3e, f). However, re-expression of S325A, S430A or S325/430A mutants in Miro2 knocked-down cells failed to complement the defective Parkin translocation upon CCCP treatment, indicating that the Parkin translocation is also critically dependent on phosphorylation at S325/S430 sites (Fig. 3e, f). Therefore, phosphorylation of Miro2 at S325/S430 by PINK1 is crucial for both the realignment of Miro2 and subsequent Parkin translocation to damaged mitochondria.

3.4. Ca^{2+} binding to the Miro2 EF2 domain regulates Parkin translocation

Miro2 contains two EF hand domains, which are known to be Ca^{2+} binding motifs. Since our data support a critical role of Miro2 in Parkin translocation during CCCP-induced mitochondrial damage, we wondered if EF hand domains play important roles in Parkin translocation. Although deletion of the EF1 domain (ΔEF1) in Miro2 did not affect its realignment in response to CCCP treatment, deletion of the EF2 domain (ΔEF2) abolished the realignment (Fig. 4a, b). Consistently, ΔEF2 but not ΔEF1 constructs failed to induce Parkin translocation (Fig. 4c, d). To further determine the role of the EF2 domain in mitophagy, we mutated glutamic acids at 208 and 328 to lysines to eliminate the calcium-binding ability of the EF1 and EF2 domains (E208K, E328K, E208/328 K), respectively [24]. In response to CCCP treatment, the E208K mutation did not affect Miro2 realignment and Parkin translocation (Fig. 4e, h, i), whereas E328K and E208/328 K mutation disabled the realignment and Parkin translocation (Fig. 4f–i), demonstrating the important role of EF2 domain of Miro2 in regulating its realignment and subsequent Parkin translocation upon CCCP treatment.

Interestingly, compared with Miro2 overexpression-induced Parkin translocation under unperturbed conditions, co-overexpression of Miro2 mutants (ΔEF1, ΔEF2, E208K, E328K and E208/328 K) with Parkin failed to promote Parkin translocation under unperturbed conditions (Fig. 4c, d, h, i). Considering that co-expression of Miro2 and Parkin could induce reduction of mitochondrial membrane potential, we also measured the mitochondrial membrane potential in MEFs co-overexpressing EF hand mutants (ΔEF1, ΔEF2, E208K, E328K and E208/328 K) and Parkin. The results showed that these EF hand mutants (ΔEF1, ΔEF2, E208K, E328K and E208/328 K) did not affect mitochondrial membrane potential when co-expressed with Parkin (Fig. S4a online). In addition, Miro2 EF hand mutants (ΔEF1, ΔEF2, E208K, E328K and E208/328 K) clearly lessened Miro2 interaction with Parkin (Fig. S4b online).

CCCP or FCCP treatment can result in mitochondrial membrane potential collapse and rapid Ca^{2+} efflux from mitochondria [37,38], hinting that mitochondrial Ca^{2+} efflux may play an important role at the early stage of mitophagy. Considering that Miro2 EF2 hand domain mutants (ΔEF2 and E328K) inhibit CCCP-induced Parkin translocation, we then used BAPTA-AM to chelate cytoplasmic Ca^{2+} to test the effects of Ca^{2+} binding to the EF hand domain of Miro2 on Parkin translocation. Pre-treatment with BAPTA-AM prevented CCCP-induced Parkin translocation (Fig. S4c, d online), indicating that Ca^{2+} efflux from mitochondria during CCCP-induced depolarization is essential for Miro2-mediated Parkin translocation. Ruthenium Red, a hexavalent polysaccharide stain, is a non-competitive inhibitor of mitochondrial Ca^{2+} uniporter (MCU) which can abolish Ca^{2+} influx into mitochondria [39–41]. Pre-treatment with Ruthenium Red did not affect CCCP-induced Parkin translocation (Fig. S4e online), suggesting that Ca^{2+} influx into mitochondria is not essential for Parkin translocation. Mitochondrial permeability transition pore (mPTP) and mitochondrial Na^{+}/Ca^{2+} exchanger (NCXL) have been reported to be mitochondrial Ca^{2+} efflux routes [37,42–49]. Pretreatment with mPTP inhibitor cyclosporin A (CsA) or Bongrekic acid (BA), and NCXL inhibitor CPG37157 did not affect CCCP-induced Parkin translocation (Fig. S4f–h online), suggesting that other mPTP and NCXL-independent mitochondrial Ca^{2+}-releasing mechanism(s) were induced by CCCP. Above all, these results demonstrate that Ca^{2+} binding to the EF2 domain of Miro2 is required for Parkin translocation during mitophagy.

3.5. Parkin translocation is not dependent on the GTPase activities of Miro2

To evaluate the role of GTPases activity in mitophagy, we next made deletions of GTPase1 domain (ΔGTPase1) and GTPase2 domain (ΔGTPase2) in Miro2. In response to CCCP treatment, ΔGTPase1 did not affect its realignment whereas ΔGTPase2 abolished its realignment (Fig. S5a, b online). Accordingly, ΔGTPase1 did not affect Parkin translocation while ΔGTPase2 did (Fig. S5c, d online). The GTPases are a large family of hydrolase enzymes, which bind and hydrolyze guanosine triphosphate (GTP). GTPases are activated when binding with GTP but inactivated when bound to GDP. We next wanted to know whether activation or inactivation of the Miro2 GTPase activity affects Miro2 realignment. Mutations at threonine 18 and serine 430 to asparagine have been reported to inactivate GTPase activity in the first and second GTPase domain (T18N, S430N), respectively [24]. While the mutation at alanine 13 and arginine 425 to valine made Miro2 constitutively active in the first and second GTPase domain (A13V, R425V) [24]. Consistent with the above ΔGTPase1 results, inactivation of GTPase1 (T18N and A13V mutation) did not affect the realignment of Miro2 (Fig. 5a, d) and subsequent Parkin translocation (Fig. 5g–j) upon CCCP treatment. Interestingly, GTPase2 inactivation mutations (S430N and T18N/S430N) abolished the CCCP-induced Miro2 realignment and subsequent Parkin translocation, whereas the Miro2 constitutive active mutants (R425V and A13V/R425V) did not (Fig. 5b, c, e, f). The S430N mutation inactivates the second GTPase of Miro2, and we found that S430N mutation also blocked CCCP-induced phosphorylation of Miro2 (Fig. S5e online). To clarify whether the decreased Parkin translocation is caused by GTPase2 inactivation or the un-phosphorylation of Miro2, we used Rho GTPase inhibitor Rhosin to inhibit GTPase activity in order to exclude the

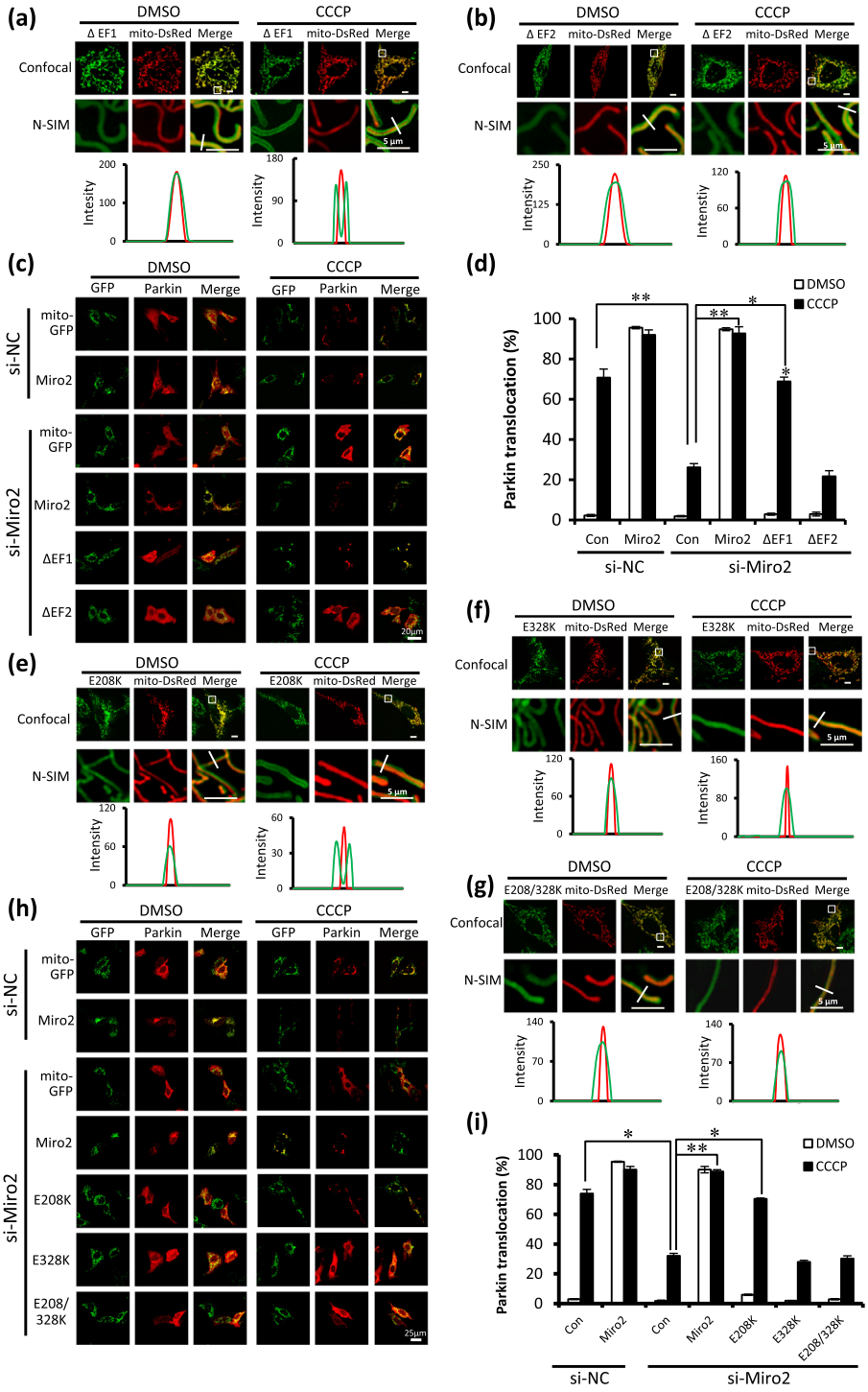

Fig. 4. The EF2 domain of Miro2 is crucial for Parkin translocation (a and b) ΔEF2 abolishes the Miro2 realignment in response to CCCP treatment. MEFs co-expressing mito-DsRed and GFP-Miro2-ΔEF1 or GFP-Miro2-ΔEF2 were imaged within 1 h after treatment with DMSO or 20 μmol/L CCCP. Note that the fluorescence images from different channels may have shifted due to that confocal and N-SIM imaging having been done in living cells, in which the mitochondria are very mobile. The fluorescence intensity profiles were taken across the area indicated by the white line in N-SIM images. (c and d) ΔEF2 eliminates Parkin translocation. Miro2 knocked-down MEFs were co-expressed with DsRed-Parkin and mito-GFP, GFP-Miro2-ΔEF1 or GFP-Miro2-ΔEF2, and treated with 20 μmol/L CCCP for 6 h. Complete overlap of DsRed-Parkin with GFP was considered to represent Parkin translocation. Miro2 coding sequence has been changed (without changing amino acid sequence) and thus resistant to siRNA against Miro2. (e–g) Mutation at glutamate 328 abolishes the Miro2 realignment in response to CCCP treatment. MEFs co-expressing mito-DsRed and GFP-Miro2-E208K, GFP-Miro2-E328K or GFP-Miro2-E208/328 k were treated with DMSO or 20 μmol/L CCCP and then imaged within 1 h. Note that the fluorescence images from different channels may have shifted due to confocal and N-SIM images having been acquired on living cells, in which the mitochondria are very mobile. The fluorescence intensity profiles were taken across the area indicated by the white line in N-SIM images. (h and i) Mutation at glutamate 328 eliminates Parkin translocation. Miro2 knocked-down MEFs were co-expressed with DsRed-Parkin and mito-GFP, GFP-Miro2-E208K, GFP-Miro2-E328K or GFP-Miro2-E208/328 K, and treated with 20 μmol/L CCCP for 6 h. Complete overlap of DsRed-Parkin with GFP was considered to represent Parkin translocation. Miro2 coding sequence has been changed (without changing amino acid sequence) and thus resistant to siRNA against Miro2. $^{*}P < 0.05$, $^{**}P < 0.01$. Data are from three independent experiments and the results are presented as mean ± SEM.

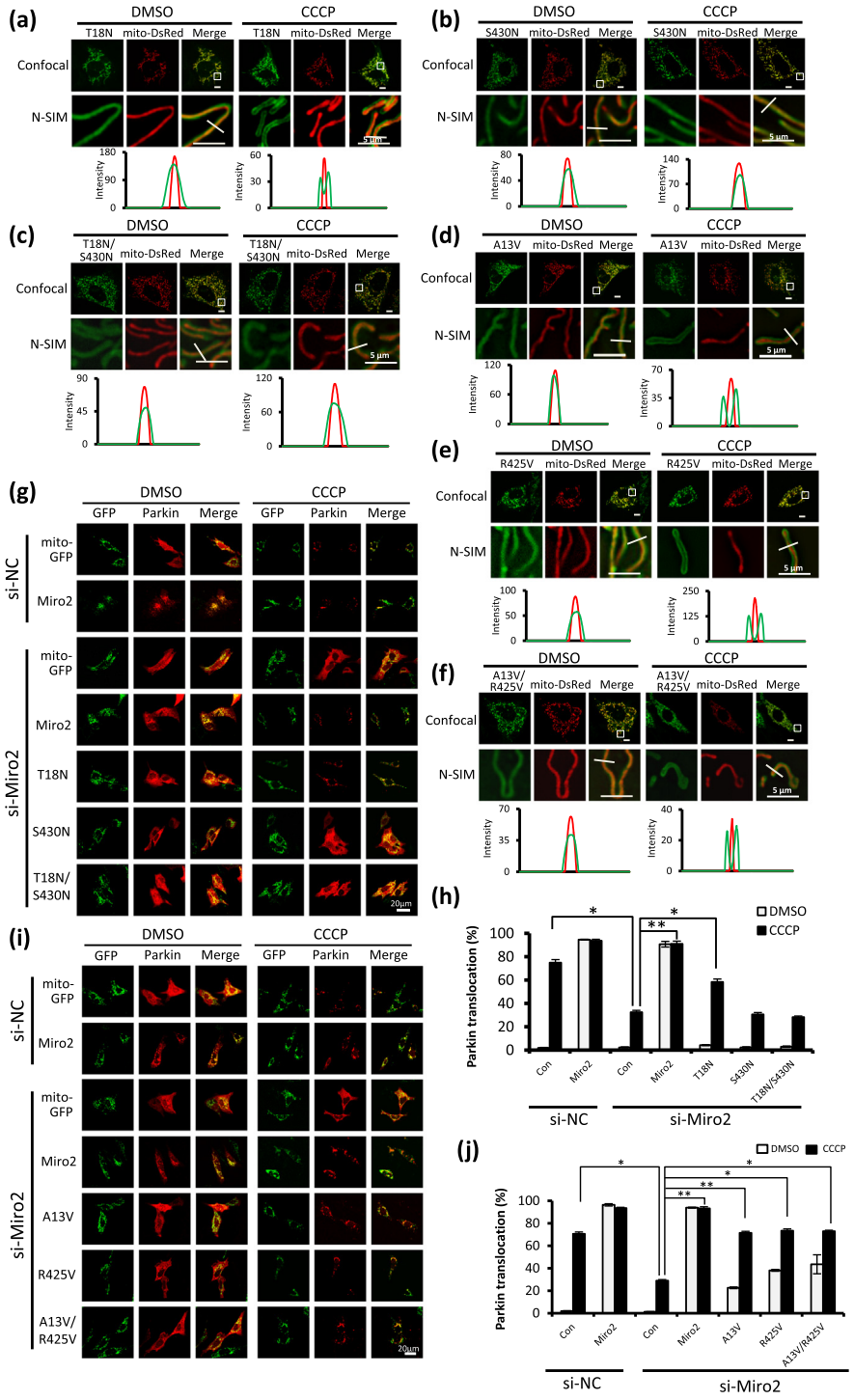

Fig. 5. Parkin translocation is not dependent on the GTPase activity of Miro2 (a–c) The mutation S430N disables Miro2 realignment. MEFs co-expressing mito-DsRed and GFP-Miro2-T18N, GFP-Miro2-S430N or GFP-Miro2-T18N/S430N were treated with DMSO or 20 μmol/L of CCCP and then imaged within 1 h. Since the images were acquired from living cells, the fluorescence shifts induced by mitochondrial mobility may be observed in pairs of confocal and N-SIM images of Confocal and N-SIM. The fluorescence intensity profiles were taken across the area indicated by the white line in N-SIM images. (d–f) The activation of Miro2 GTPase domains does not affect their realignment. MEFs co-expressing mito-DsRed and GFP-Miro2-A13V, GFP-Miro2-R425V, or GFP-Miro2-A13V/R425V were treated with DMSO or 20 μmol/L CCCP and then imaged within 1 h. Please note that the fluorescence images may shift slightly since the confocal and N-SIM imaging is acquired in living cells. The fluorescence intensity profiles were taken across the area indicated by the white line in N-SIM images. (g and h) The inactivation of the GTPase2 domain lessens Parkin translocation. Miro2-depleted MEFs were co-expressed with DsRed-Parkin and mito-GFP, GFP-Miro2-T18N, GFP-Miro2-S430N or GFP-Miro2-T18N/S430N, and treated with 20 μmol/L CCCP for 6 h. Miro2 coding sequence has been changed (without changing amino acid sequence) and thus resistant to siRNA against Miro2. (i and j) The activity of Miro2 GTPase domains does not affect Parkin translocation. Miro2 knocked-down MEFs were co-expressed with DsRed-Parkin and mito-GFP, GFP-Miro2-A13V, GFP-Miro2-R425V, or GFP-Miro2A13V/R425V, and treated with 20 μmol/L CCCP for 6 h. Miro2 coding sequence has been changed (without changing amino acid sequence) and thus resistant to siRNA against Miro2. $^{*}P < 0.05$, $^{**}P < 0.01$. Data are from three independent experiments and results are presented as mean ± SEM.

effect of the Miro2 second GTPase inactivation on Parkin translocation. Rhosin can inhibit GTPase activity by preventing the interaction between Rho GTPase and its GEFs. Pretreatment with Rhosin did not affect CCCP-induced Parkin translocation (Fig. S5f online), suggesting that the lessened Parkin translocation induced by the mutation of S430 is mainly due to its inability to be phosphorylated. Moreover, GTPase mutations (T18N, S430N, A13V, R425V) also lessened their interaction with Parkin under unperturbed conditions (Fig. S5g online). Meanwhile, A13V and R425V showed a stronger interaction with Parkin than T18N and S430N, and the interaction of R425V with Parkin was decidedly stronger than A13V (Fig. S5g online). These results may explain the different effects of GTPase mutations on Parkin translocation under unperturbed conditions. Based on these results, we conclude that the GTPase activity of Miro2 is not required for Parkin translocation during mitophagy.

3.6. Miro2 mutant abolishes its realignment and subsequently suppresses Parkin translocation

Miro2 gene mutations have been observed in patients suffering from early-onset lactic acidosis. Among them, three single nucleotide polymorphisms (SNPs) result in amino acid substitutions in the protein, including c.262G > A(A88T), c.734G > A (R245Q), and c.1273C > T (R425C) (Table S1 online) [50]. Exonisation of intron 10 between exons 10 and 11, c.748_749insIN10 (Exon10), is also observed in the four patients suffering from lactic acidosis (Table S1 online) [50]. Exon10 alters the downstream reading frame and introduces premature STOP codons into the sequence, resulting in a C-terminal truncated Miro2 protein. Due to the abnormal mitochondria observed in these patients [50], we wanted to know whether these Miro2 mutant affect mitophagy. Previous reports show that Miro2 knockout animals are viable and fertile whereas Miro1 knockout animals shows postnatal lethality [51,52]. We generated Miro2$^{-/-}$ mice by deleting the region spanning from the second to the forth exons of Miro2 in zygotes using the CRISPR/Cas9 system, and isolated MEFs from day 12.5 to 13.5 postcoitum mouse embryos. A Western blot confirmed the deletion of Miro2 (Miro2-KO) (Fig. S6a online). The distributions of Miro2 mutants A88T, R245Q and R425C when expressed in WT MEFs were completely overlapped with mito-DsRed (Fig. 6a–c), whereas Exon10 resulted in loss of mitochondrial localization owing to the lack of the C-terminal transmembrane domain (Fig. 6d). In response to CCCP treatment, A88T and R425C were still able to undergo a realignment leading to relocalization (Fig. 6a, c). However, the R245Q mutant was unable to relocalized (Fig. 6b). To further determine whether these mutants were still able to induce Parkin translocation, we expressed mutants A88T, R245Q, R425C or Exon10 in Miro2-KO MEFs (Fig. 6e, f). We found that, while A88T and R425C behaved similarly to WT Miro2, R245Q and Exon10 mutants failed to induce Parkin translocation in response to CCCP assault (Fig. 6e, f). Therefore, our data indicate that some human patient-derived Miro2 mutations (Exon10, R245Q) can disable the function of Miro2 in Parkin translocation.

All four patients had exonisation of intron 10 (Exon10 mutation), and three patients had the R245Q mutation. Among them, patient "P3", whose Miro2 transcripts consisted of as much as ~50% exonisation of intron 10% and 50% of R245Q, showed the most severe lactic acidosis and died at the age of 15 months [50]. The direct correlation between Miro2 deficiency and disease severity supports an important role of Miro2 in mitochondrial health maintenance.

3.7. Miro2 deficiency results in lactic acidosis

To determine the role of Miro2 in lactic acidosis, we measured lactic acid production of Miro2-KO MEFs using the XF analyzer. Lactic acid production was indicated by the extracellular acidification rate (ECAR). Glyolytic ECAR was measured immediately following the addition of glucose. Acidification of the extracellular space in Miro2 KO MEFs occurred at a much greater rate than WT MEFs (Fig. S6b, c online). Oligomycin, an inhibitor of ATP, reduces mitochondrial respiration and maximizes glycolytic ATP production. After treatment with Oligomycin, glycolytic capacity was significantly higher in Miro2-KO MEFs than that in WT MEFs (Fig. S6b and c). An inhibitor of the first step of glycolysis, 2-deoxyglucose (2-DG), was used to confirm that the ECAR measured was resulted from glycolytic metabolism. ECAR was restored to non-glycolytic levels in both cell lines following 2-DG treatment. Reserved glycolytic capacity was observed in WT MEFs but not in Miro2-KO MEFs, further suggesting that Miro2-KO MEFs have acquired a glycolytic phenotype to satisfy ATP energetic demands (Fig. S6b, c online). Moreover, the D-lactic acid concentration in the sera Miro2-KO mice was significantly higher than that in WT mice (Fig. S6d online). To further explore the cause of lactic acid production, we next examined mitochondrial ultrastructure with a transmission electron microscopic. The results showed that deletion of Miro2 resulted in an accumulation of abnormal mitochondria (mitochondrial cristae disordering, swelling or even disappearance) (Fig. S6f, g online) manifesting the importance of Miro2 in culling the damaged mitochondria in cells.

3.8. Miro2 deficiency delays reticulocyte maturation in the peripheral blood and results in cardiac disorders

Considering the important role of autophagy in reticulocyte maturation [53–55], we next determined the role of Miro2 in this process. We first examined red blood cells (RBCs) in the peripheral blood by staining blood smears with Wright-Giemsa stain. The results showed that polychromasia was observed in 2-week-old WT, Miro2$^{+/-}$ and Miro2$^{-/-}$ mice (Fig. 7a, b). However, the percentage of polychromasia in Miro2$^{+/-}$ and Miro2$^{-/-}$ mice was significantly higher than that in WT (Fig. 7a, b). At 5 weeks of age, Miro2$^{-/-}$ mice still retained a significantly higher percentage of polychromasia than WT mice (Fig. 7a, b), indicating that Miro2 deficiency hindered the maturation of reticulocytes in the peripheral blood. To explore the cause of reticulocyte immaturity, we observed cell ultrastructure with transmission electron microscopy (TEM). Electron microscopy revealed that very few RBCs in WT and Miro2$^{+/-}$ mice at 4-week-old contained mitochondria or other organelles (Fig. 7c, d). However, obviously more RBCs preserved multiple mitochondria, ribosomes, autophagosomes (Fig. 7e, f), or even nuclei (Fig. 7g) in Miro2$^{-/-}$ mice, demonstrating that Miro2 deficiency significantly delays reticulocyte maturation.

Mitochondrial dysfunction has been implicated in a number of cardiac disorders. We next wanted to know whether Miro2 deficiency causes cardiac disorders. Compared with WT mice, the hearts of 2-month-old Miro2-KO mice were smaller (Fig. 7h, i). Myocardial histology of Miro2-deficient hearts was unremarkable, and lipofuscin was not observed (Fig. 7h, i and l). However, Cardiac dilatation was obviously seen in the Miro2-KO hearts at 11-month-old (Fig. 7j, k), and myocardial histology showed that the myocardial fibers became significantly thicker in Miro2-KO hearts (Fig. 7j–l). Though the hearts from 6-month-old Miro2-KO mice exhibited either smaller size (KO-1) or dilatation (KO-2), the number of mitochondria was essentially the same in the mutant cardiomyocytes compared with WT (Fig. 7m–p, WT: Fig. 7m; KO: Fig. 7n, o). How-

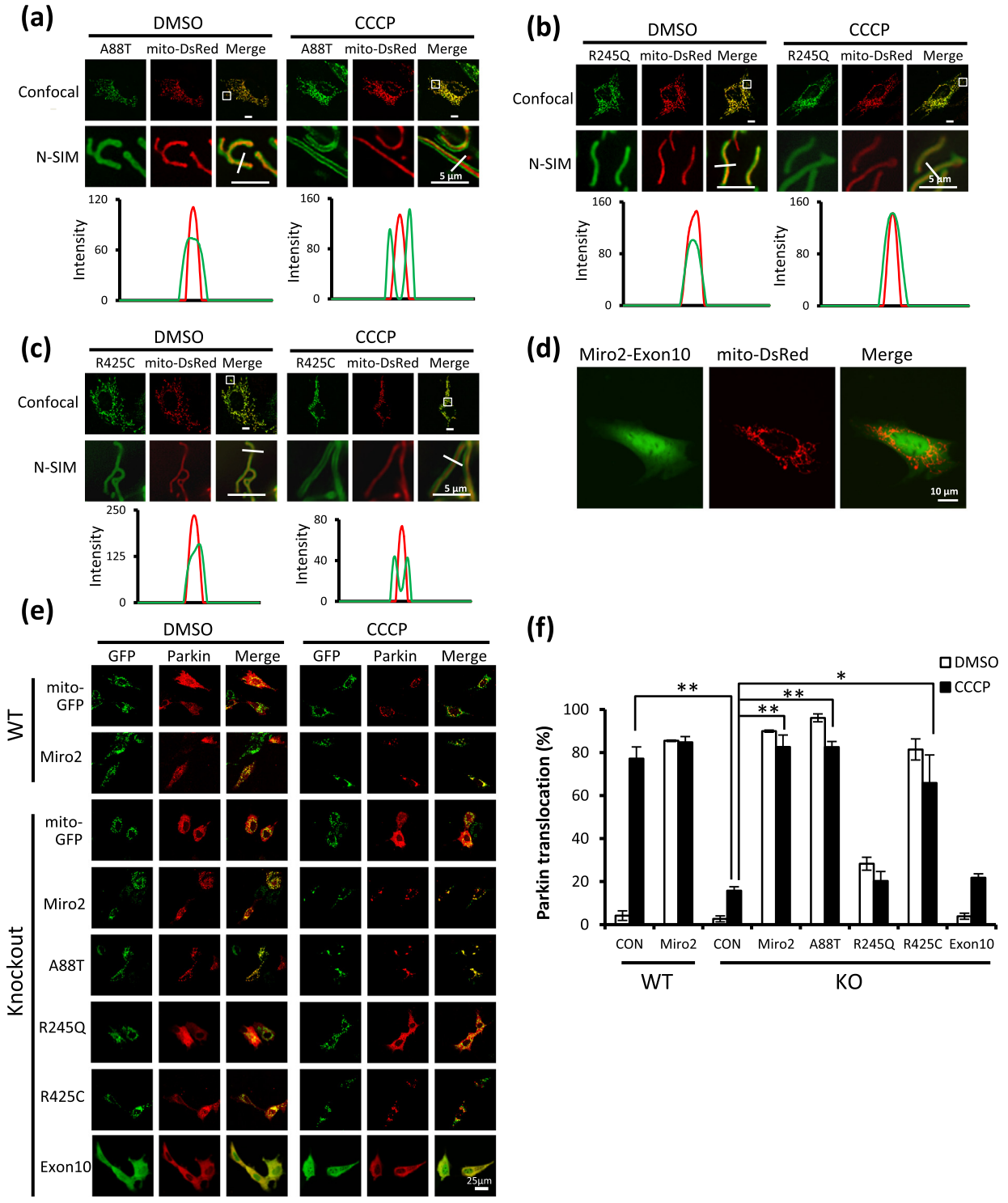

Fig. 6. Human Miro2 mutants exhibit inhibited realignment and subsequently suppress Parkin translocation. (a) Representative images showing the realignment of GFP-Miro2-A88T in response to CCCP treatment. MEFs co-expressing mito-DsRed and GFP-Miro2-A88T were treated with DMSO or 20 μmol/L of CCCP and then imaged within 1 h. Note that the fluorescence images from different channels may have shifted since confocal and N-SIM imaging is done on living cells, in which the mitochondria are very mobile. The fluorescence intensity profiles were taken across the area indicated by the white line in N-SIM images. (b) Representative images showing the co-localization of GFP-Miro2-R245Q with mito-DsRed. Similar experiments as (a) were done with a GFP-Miro2-R245Q mutant. No realignment of GFP-Miro2-R245Q was observed in response to CCCP treatment. The fluorescence intensity profiles were taken across the area indicated by the white line in N-SIM images. (c) Representative images showing the realignment of GFP-Miro2-R425C in response to CCCP treatment. Similar experiments as were done in (a) with a GFP-Miro2-R425C mutant. The fluorescence intensity profiles were taken across the area indicated by the white line in N-SIM images. (d) Representative images showing that Miro2-Exon10 fails to co-localize with mitochondria. Similar experiments were done in (a) with a GFP-Miro2-Exon10 mutant. GFP-Miro2-Exon10 and mito-DsRed were co-overexpressed in MEFs, and images were acquired on the next day. GFP-Miro2-Exon10 does not co-localize with mitochondria. (e and f) Miro2 R245Q and Exon10 mutants fail to recruit Parkin in response to CCCP treatment. Miro2 knockout MEFs were co-expressed with DsRed-Parkin and mito-GFP, GFP-Miro2, GFP-Miro2-A88T, GFP-Miro2-R245Q, GFP-Miro2-R425C or GFP-Miro2-Exon10, and treated with 20 μmol/L of CCCP for 6 h. Complete overlap of DsRed-Parkin with GFP was considered to represent Parkin translocation. Miro2 coding sequence has been changed (without changing amino acid sequence) and thus resistant to siRNA against Miro2. $^{*}P < 0.05$, $^{**}P < 0.01$. Data are from three independent experiments and the results are presented as mean ± SEM.

ever, the amount of abnormal mitochondria was obviously increased in cardiomyocytes of Miro2-KO mice compared with WT mice (Fig. 7m–o, q, WT: Fig. 7m; KO: Fig. 7n, o). Therefore, Miro2 deficiency leads to a defect in the removal of damaged mitochondria and to the accumulation of abnormal mitochondria in cardiac myocytes, thus further causing cardiac disorder.

4. Discussion

Selective recognition and clearance of dysfunctional mitochondria by mitophagy are central to the mitochondrial quality control system. Parkin translocation to damaged mitochondria constitutes the initiation step of mitophagy. Before translocating to mitochondria, Parkin is able to be activated by phosphorylated ubiquitin in addition to its phosphorylation by PINK1. Since ubiquitin phosphorylation by PINK1 takes place in the vicinity of the mitochondrial outer membrane, Parkin likely translocates proximal to the mitochondrial outer membrane in order to be activated by PINK1. Therefore, it is highly likely there are mitochondrial outer membrane proteins supplying the platform for Parkin activation. In the present study, we propose a model for how Miro2 functions as a platform for Parkin recognition and translocation to damaged mitochondria. Under unperturbed conditions, PINK1 is cleaved by PARL at mitochondrial inner membrane [5,6]. Upon mitochondrial membrane potential collapse, Miro2 is quickly phosphorylated at Ser325/Ser430 by the full-length PINK1 after PINK1 translocates to the mitochondrial outer membrane. Meanwhile, Ca^{2+} efflux from the mitochondria is sensed by the EF2 hand domain of Miro2. When Miro2 is phosphorylated by PINK1 and binds with Ca^{2+} released from mitochondria, Miro2 undergoes a realignment and demultimerization from tetramers to monomers on the mitochondrial outer membrane. Then the realigned Miro2 acts as a platform for Parkin recognition, translocation, and subsequent initiation of mitophagy. Thus, Miro2 functions as a Parkin platform which is able to detect both membrane potential collapse and Ca^{2+} release from damaged mitochondria to ensure that only damaged mitochondria are recognized and targeted by Parkin for mitophagic clearance. Disease mutant Miro2 proteins (such as exonisation of intron 10−Exon 10, R245Q) are disrupted in their ability to recruit Parkin to damaged mitochondria, leading to defects in the clearance of damaged mitochondria and accumulation of abnormal mitochondria, which might be causal in lactic acidosis and cardiac disorders.

Unlike *Drosophila*, which has only one Miro isoform (dMiro), there are two isoforms in mammals, Miro1 and Miro2. In *Drosophila,* dMiro regulates mitochondrial mobility by forming a complex with Milton and kinesin-1 heavy chain (KHC) [56,57], providing a link between mitochondria and the trafficking apparatus of the microtubules [24,58]. In agreement with the function of dMiro in mitochondrial mobility, Miro1 and Miro2 have also been reported to be involved in mitochondrial mobility [28,59]. Miro1 and Miro2 are degraded by PINK1/Parkin to arrest mitochondrial mobility in response to CCCP [28]. However, their lifetimes are distinct, with Miro1 being degraded rapidly, while Miro2 levels are maintained over a long duration [28]. Consistent with a previous report [28], we also found that Miro2 is degraded minimally upon CCCP treatment (Fig. 1h). By using super-resolution microscopy (the N-SIM system), we show that Miro2 (but not Miro1) forms a clear thin layer surrounding mito-DsRed (Fig. 1a, b), suggesting that Miro2 is realigned upon CCCP treatment causes it to relocalize. Results obtained with the chemical cross-linker DSS further support that Miro2 molecules undergo re-organization of their quaternary structure on the mitochondrial outer membrane (Figs. S1d, S3g online). Interesting, Miro2 overexpression with Parkin decreases mitochondrial membrane potential even without CCCP assault, thus leading to realignment of Miro2 and subsequent Parkin translocation (Fig. S2a, b online). Moreover, Miro2 deficiency significantly diminishes the degradation of mitochondrial proteins (Fig. 1h, Fig. S2c online). Together, these results support an important role of Miro2 in mitophagy. Recently, Miro1 proteins, also possible Miro 2 proteins, have been reported to prime mitochondria for Parkin translocation and mitophagy [60,61], highlighting the importance of Miro proteins for Parkin transloaction and mitophagy.

In response to CCCP treatment, the interaction between Miro2 and PINK1 is markedly increased, and Miro2 phosphorylation levels peaked at 0.5–1 h (Fig. 2). Different from the reported Miro1 phosphorylation sites of at Ser156, 298 and 299, we have demonstrated that Miro2 is phosphorylated by PINK1 at Ser325 and Ser430 both in vitro and in vivo (Fig. 2). Mutation of either Ser325 or Ser430 to alanine prevents Miro2 realignment and subsequent Parkin translocation (Fig. 3), indicating that Miro2 phosphorylation is an essential feature enabling Parkin translocation. Interestingly, the realignment of Miro2 and the subsequent Parkin translocation to damaged mitochondria are critically dependent on PINK1-mediated phosphorylation at Ser325/Ser430, and on Ca^{2+} binding to the EF2 domain. Miro2 mutations that disable its realignment (Ser325, Ser430A, Ser325/Ser430A, ΔEF2, E328K, R245Q, Exon10) also blocks the Parkin translocation to CCCP-damaged mitochondria, indicating that the realigned Miro2 could act as a platform for Parkin translocation. Though phosphomimetic mutant Miro1 S156E has been shown to increase Parkin and ubiquitin co-localization to mitochondria, the S156E mutation does not cause LC3 recruitment and further decrease of mitochondrial content compared with Miro1 co-expression with Parkin, suggesting that Miro1 S156E does not induce mitophagy [60]. In addition, the phosphomimetic mutants Miro1 T298/299E only render Miro1 resistant to Parkin-induced ubiquitination and degradation [60]. Therefore, Miro1 phosphorylation at S156 or T298/T299 may only be in favor of regulating mitochondrial mobility by affecting Miro1 degradation [29,60]. However, there is a controversy about Miro1 phosphorylation [28,29,60]. Our Phos-tag™ SDS-PAGE results indicate that Miro1 phosphorylation is not detectable within 1 h after CCCP treatment (Fig. 2d). The discrepancy might be due to the different experimental conditions such as cell lines and different CCCP treatment time.

In addition to PINK1-mediated Miro2 phosphorylation, Ca^{2+} binding to Miro2 is also required for Parkin translocation. CCCP or FCCP treatment immediately results in an elevation of cytoplasmic Ca^{2+} and a rapid Ca^{2+} efflux from mitochondria [37,38,62], which may enhance Ca^{2+}-induced arrest of mitochondrial mobility in Miro2 overexpressed cells. In this study, we found that EF2 deletion (ΔEF2), or point mutation (E328K), either of which abolish the Ca^{2+} binding ability of the EF2 hand domain, prevented Miro2 realignment and Parkin translocation (Fig. 4). Whereas EF1 deletion (ΔEF1) or site mutation (K208) of Miro2 do not affect its realignment and subsequent Parkin translocation (Fig. 4). Furthermore, BAPTA-AM pretreatment significantly decreased Parkin translocation induced by CCCP treatment (Fig. S4c, d online), indicating that Ca^{2+} binding to the EF2 domain is essential for Parkin translocation as well. However, it is not clear which protein(s) is

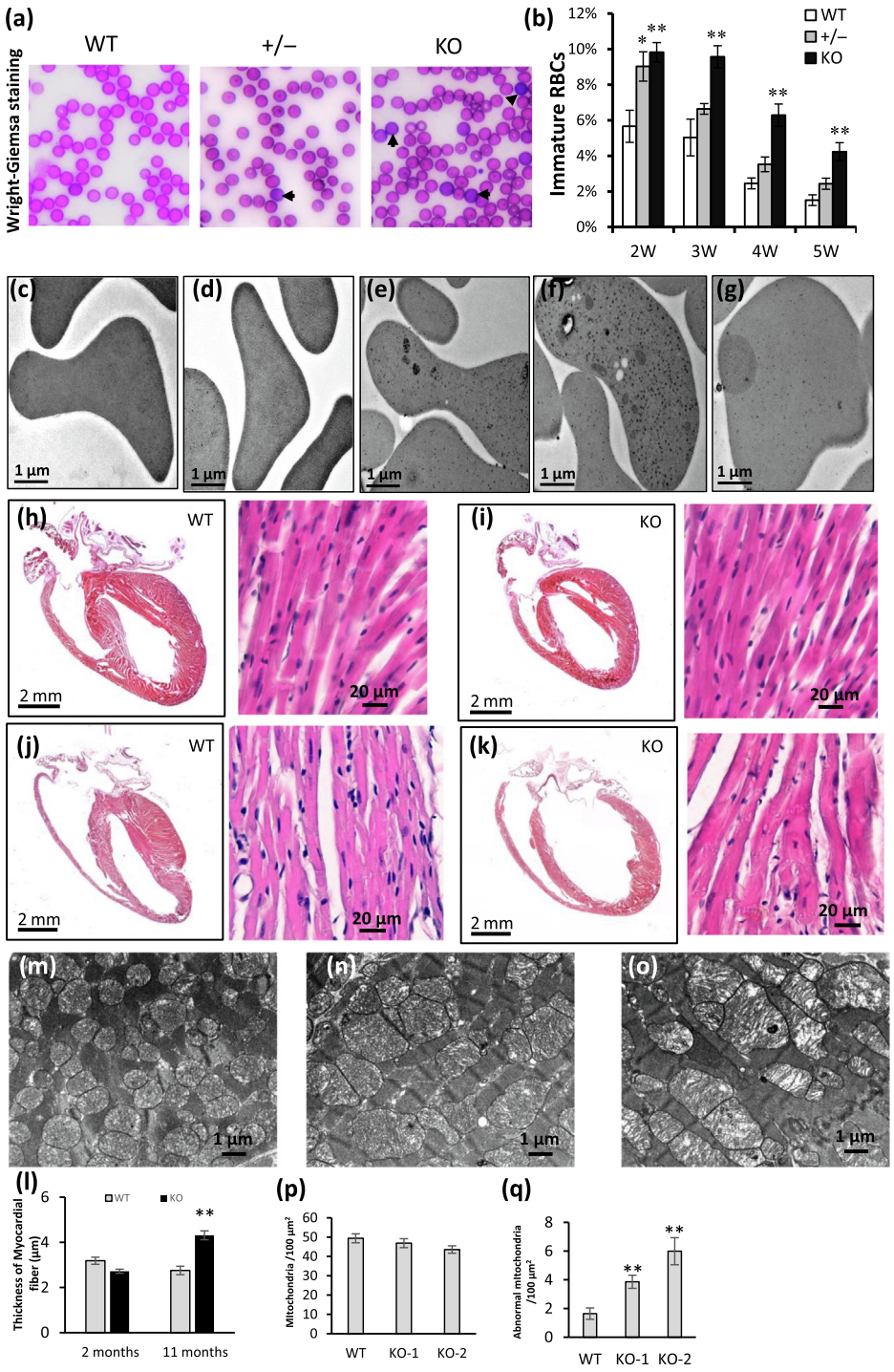

Fig. 7. Miro2 deficiency delays reticulocyte maturation in the peripheral blood and results in cardiac disorder. (a, b) Representative images of blood smears from WT, Miro2$^{+/-}$ and Miro2 KO mice. The blood smears of red blood cells (RBCs) in the peripheral blood from WT (n = 5), Miro2$^{+/-}$ (n = 6) and Miro2 KO (n = 7) mice were stained with Wright-Giemsa. Statistical analysis shows that reticulocyte maturation in the peripheral blood is delayed in Miro2 KO mice (b). The arrow indicates the immature RBCs. (c, d) Transmission electron microscopy (TEM) showing erythrocytes in the peripheral blood of 4-week-old WT mice (c) and Miro2$^{+/-}$ (d) mice. (e–g) TEM showing erythrocytes in the peripheral blood of Miro2 KO mice. Ribosomes (e), mitochondria (f), autophagosomes (f) or even nucleius (g) are observed in the peripheral blood of Miro2 KO mice. (h, i) Representative hearts, histological sections from 2-month-old WT and Miro2 KO mice. (j, k) Representative hearts, histological sections from 11-month-old WT and Miro2 KO mice. (l) The thickness of myocardial fiber of 11-month-old Miro2 KO mice is significantly increased. (m) TEM showing normal cardiomyocyte mitochondria from 6-month-old WT mice. (n, o) TEM showing abnormal cardiomyocyte mitochondria from 6-month-old KO mice. Mitochondria become obviously enlarged in KO mice regardless of whether the heart size becomes smaller (n) or dilatated (o). (p) The number of mitochondria shows no detectable change in cardiomyocytes of smaller (KO-1) and dilatated (KO-2) hearts from 6-month-old KO mice. The data was acquired from more than 10 TEM images of WT, KO-1, or KO-2. (q) The number of abnormal mitochondria is significantly increased in cardiomyocytes of smaller (KO-1) and dilatated (KO-2) hearts from 6-month-old KO mice.

responsible for mitochondrial Ca^{2+} efflux during CCCP-induced mitochondrial depolarization, which warrants further investigations. Since both PINK1-mediated Miro2 phosphorylation and Ca^{2+} binding to Miro2 are essential for CCCP-induced Parkin translocation, the accuracy of mitophagy could be achieved by detecting both membrane potential collapse and Ca^{2+} efflux from damaged mitochondria via Miro2.

In our study we found that co-overexpression of Miro2 and Parkin significantly decrease mitochondrial membrane potential to ~60% (Fig. S2a, b online). However, co-overexpression of Parkin with either Miro1 or Miro2 mutants (ΔEF1, ΔEF2, E208K, E328K) does not reduce mitochondrial membrane potential (Fig. S4a online). Moreover, Miro2 mutants (ΔEF1, ΔEF2, E208K and E328K) show obviously decreased interactions with Parkin (Fig. S4b online). Together, these results may explain the decreased Parkin translocation induced by Miro2 EF hand mutations (ΔEF1, ΔEF2, E208K, E328K) under unperturbed conditions (Fig. 4c, d, h, i). Similar to what was observed with EF hand mutations in Parkin translocation, GTPase domain mutations (A13V, R425V, T18N and S430N) also show decreased Parkin translocation under unperturbed conditions (Fig. 5g–j). T18N and S430N inactivate GTPase activity in the first and second GTPase domains, respectively, while A13V and R425V make Miro2 constitutively active in the first and second GTPase domains [24]. Our results show that Miro2 GTPase mutants exhibited decreased interactions with Parkin (Fig. S5g online), which explains the molecular basis for the differences in Parkin translocation between WT Miro2 and Miro2 mutants (Fig. 5g, j). Moreover, the interaction of Parkin with A13V or R425V is obviously stronger than that with T18N or S430N, which explains the higher percentage of cells with Parkin translocation under unperturbed conditions in cells expressing RHOT2 A13V and R425V. Notably, S430 in Miro2 is one of the PINK1 phosphorylation sites (Fig. 2e, g, h; Fig. S5e online). Based on our data, S430 phosphorylation by PINK1 is essential for the realignment of Miro2 and subsequent Parkin translocation (Fig. 3b, e and f). S430N mutation abrogates phosphorylation of Miro2 at 430 site by PINK1 (Fig. S5e online). This could explain why S430N mutation has a low percentage of Parkin translocation under unperturbed conditions.

Parkin activation and translocation to damaged mitochondria is believed to be the first step of mitophagy for the selective clearance of damaged mitochondria. Upon mitochondria membrane potential collapse, Parkin is activated by PINK1 [17,18]. Parkin can alternatively be activated by PINK1-phosphorylated ubiquitin [11,12,19]. Due to the occurrence of ubiquitin phosphorylation in the vicinity of the mitochondrial outer membrane, it is logiacl the Parkin would translocate proximal to mitochondrial outer membrane in order to be activated [11]. Therefore, it is reasonable to expect there might be mitochondrial outer membrane proteins that function as a platform for both ubiquitin phosphorylation and Parkin activation [11]. MFN2, a mitochondrial outer membrane protein that mediates mitochondrial fusion, has been shown to be a substrate of PINK1 and a receptor for Parkin recruitment [10], suggesting that MFN2 could be a platform for Parkin recruitment. In addition, Voltage-dependent anion channels (VDACs) can also recruit Parkin to defective mitochondria to promote mitochondrial autophagy [63], though there is inconsistency about the roles of VDACs in mitophagy [1,63,64]. Dysfunctional mitochondria undergo multiple changes, such as depolarization and Ca^{2+} efflux. Therefore, it is likely important for mitochondrial outer membrane proteins to detect multiple simultaneous signals from damaged mitochondria to ensure the accuracy of mitophagy. In this study, we find that Miro2 is phosphorylated by PINK1 upon mitochondrial membrane potential collapse (Fig. 2). Moreover, Miro2 is able to sense Ca^{2+} efflux from mitochondria via its EF2 hand domain (Fig. 4). After being phosphorylated and sensing Ca^{2+} efflux from mitochondria, Miro2 undergoes a realignment, which creates a platform for ubiquitin phosphorylation and Parkin activation, which in turn triggers Parkin recognition and translocation. Importantly, the realignment of Miro2 is strictly regulated, which ensures the precise regulation of mitophagy.

Heart failure is one of the most common causes of mortality and morbidity in the world whereas PD patients have most frequently heart failure. The prevalence of heart failure has been found to be twice as high among PD patients compared with overall population regardless of any other heart or cardiovascular disease risk factors [65]. PD is significantly associated with increased concentric left ventricular hypertrophy and diastolic dysfunction, and advanced stages of PD are associated with a more severe cardiac affection [66], which may explain the higher prevalence of heart failure in PD patients. As a mouse model of PD, PINK1 KO mice also showed left ventricular dysfunction and cardiac hypertrophy [67]. Additionally, as the substrate of PINK1, MFN2 ablation also induced cardiac dysfunction [10]. Though cardiac disorder is not observed in a Parkin knockout mouse model [68], cardiomyocyte mitochondria of these Parkin null mice were smaller and less organized than that of WT type mice, and developed abnormal electron dense inclusions over time [69]. Therefore, PINK1 and Parkin knockout mice mimic the cardiac disorder of PD patients to an extent. In our study, we have found that Miro2 knockout mice show evidence of cardiac disorder (Fig. 7). Miro2 loss results in acardiotrophia at a young age which develops into dilated cardiomegaly (Fig. 7h–k). Moreover, the mitochondria become dramatically enlarged in Miro2-KO myocardia regardless of the size of the heart (smaller or dilated) (Fig. 7n, o, q). Therefore, we believe that Miro2 loss-induced defects in PINK1/Parkin dependent mitophagy could be the potential cause of cardiac disorder in Miro2 KO mice.

Mitochondrial genomes with deleterious mutations are a cause of severe inherited syndromes, such as lactic acidosis. Patients with sporadic PD have a greater number of functionally deleterious mtDNA mutations compared with age-matched controls [70,71]. Moreover, PD patients show reduced activity of the mitochondrial complex I [72,73]. These results indicate that PD patients may suffer from lactic acidosis. Later on, Bowen et al. determined that there was an increase in cerebral lactate in patients with PD [74]. Recently, increased lactate was observed in larva of Drosophila mutant in Parkin [75], and PINK1 or Parkin knockout mice (mouse models of PD) have also been shown to be hyperlactatemic [76]. In our study, we have detected the elevated lactate in sera of Miro2 knockout mice, suggesting that Miro2 loss-induced defects in PINK1/Parkin dependent mitophagy could be a cause of elevated lactate in Miro2 KO mice.

Conflict of interest

The authors declare that they have no conflict of interest.

Acknowledgments

We thank Professor Hongyue Wang from the Chinese Academy of Medical science and Peking Union Medical College for providing the statistic method of the thickness of myocardial fibers, Professor Xin Pan from National Center of Biomedical Analysis and Professor Quan Chen from Institute of Zoology, Chinese Academy of Sciences for providing mitoKeima plasmid, Professor Paula L. Fischhaber at California State University Northridge for proofreading the manuscript. This work was supported by the National Natural Science Foundation of China (91754204) the Strategic Priority Research Program of the Chinese Academy of Sciences (XDA16010107), National Key Research and Development Program of China (2018YFA0108500, 2017YFC1001001), the National Natural

Science Foundation of China (81630078, 31670822, 31401151, 31570816, 81371415), the Natural Science Foundation of Beijing (5181001); CAS Strategic Priority Research Program (XDB14030300), the State Key Laboratory of Membrane Biology, and the Key Laboratory of Genomic and Precision Medicine.

Authors contribution

J. W. and S. Z. observed that Miro2 could recruit Parkin translocation and carried out most of the biochemistry experiments. Y. W. and F. W. designed and carried out all electron microscopy analysis. C. A., D. J. and L. G. designed and carried out all the Western blotting and IP experiments. Y. T. and X. Z. identified that the phosphorylation sites of Miro2 by PINK1 with some help from Y. W. and H. L.. J. G. and Z. S. maintained the Miro2 KO mouse colony. X. W., K. Y., and L. L. analysed and organized the data. T. T. and C. G. supervised the study and the manuscript writing.

Appendix A. Supplementary data

Supplementary data to this article can be found online at https://doi.org/10.1016/j.scib.2019.04.033.

References

[1] Geisler S, Holmstrom KM, Skujat D, et al. Pink1/parkin-mediated mitophagy is dependent on vdac1 and p62/sqstm1. Nat Cell Biol 2010;12:119–U170.
[2] Narendra D, Tanaka A, Suen DF, et al. Parkin is recruited selectively to impaired mitochondria and promotes their autophagy. J Cell Biol 2008;183:795–803.
[3] Youle RJ, Narendra DP. Mechanisms of mitophagy. Nat Rev Mol Cell Biol 2011;12:9–14.
[4] Beilina A, Van Der Brug M, Ahmad R, et al. Mutations in pten-induced putative kinase 1 associated with recessive parkinsonism have differential effects on protein stability. Proc Nat Acad Sci USA 2005;102:5703–8.
[5] Deas E, Plun-Favreau H, Gandhi S, et al. Pink1 cleavage at position a103 by the mitochondrial protease parl. Hum Mol Genet 2011;20:867–79.
[6] Jin SM, Lazarou M, Wang CX, et al. Mitochondrial membrane potential regulates pink1 import and proteolytic destabilization by parl. J Cell Biol 2010;191:933–42.
[7] Narendra DP, Jin SM, Tanaka A, et al. Pink1 is selectively stabilized on impaired mitochondria to activate parkin. PLoS Biol 2010;8:e1000298.
[8] Kondapalli C, Kazlauskaite A, Zhang N, et al. Pink1 is activated by mitochondrial membrane potential depolarization and stimulates parkin e3 ligase activity by phosphorylating serine 65. Open Biol 2012;2:120080.
[9] Okatsu K, Oka T, Iguchi M, et al. Pink1 autophosphorylation upon membrane potential dissipation is essential for parkin recruitment to damaged mitochondria. Nat Commun 2012;3:1016.
[10] Chen Y, Dorn GW. Pink1-phosphorylated mitofusin 2 is a parkin receptor for culling damaged mitochondria. Science 2013;340:471–5.
[11] Kane LA, Lazarou M, Fogel AI, et al. Pink1 phosphorylates ubiquitin to activate parkin e3 ubiquitin ligase activity. J Cell Biol 2014;205:143–53.
[12] Koyano F, Okatsu K, Kosako H, et al. Ubiquitin is phosphorylated by pink1 to activate parkin. Nature 2014;510:162–6.
[13] Lai YC, Kondapalli C, Lehneck R, et al. Phosphoproteomic screening identifies rab gtpases as novel downstream targets of pink1. EMBO J 2015;34:2840–61.
[14] Lazarou M, Sliter DA, Kane LA, et al. The ubiquitin kinase pink1 recruits autophagy receptors to induce mitophagy. Nature 2015;524:309–14.
[15] Shiba-Fukushima K, Arano T, Matsumoto G, et al. Phosphorylation of mitochondrial polyubiquitin by pink1 promotes parkin mitochondrial tethering. PLoS Genet 2014;10:e1004861.
[16] Stolz A, Dikic I. Pink1-parkin interplay: down to ubiquitin phosphorylation. Mol Cell 2014;56:341–2.
[17] Iguchi M, Kujuro Y, Okatsu K, et al. Parkin-catalyzed ubiquitin-ester transfer is triggered by pink1-dependent phosphorylation. J Biol Chem 2013;288:22019–32.
[18] Shiba-Fukushima K, Imai Y, Yoshida S, et al. Pink1-mediated phosphorylation of the parkin ubiquitin-like domain primes mitochondrial translocation of parkin and regulates mitophagy. Sci Rep 2012;2:1002.
[19] Kazlauskaite A, Kondapalli C, Gourlay R, et al. Parkin is activated by pink1-dependent phosphorylation of ubiquitin at ser(65). Biochem J 2014;460:127–39.
[20] Gao F, Chen D, Si JM, et al. The mitochondrial protein bnip3l is the substrate of park2 and mediates mitophagy in pink1/park2 pathway. Hum Mol Genet 2015;24:2528–38.
[21] Tanaka A, Cleland MM, Xu S, et al. Proteasome and p97 mediate mitophagy and degradation of mitofusins induced by parkin. J Cell Biol 2010;191:1367–80.
[22] Fransson A, Ruusala A, Aspenstrom P. Atypical rho gtpases have roles in mitochondrial homeostasis and apoptosis. J Biol Chem 2003;278:6495–502.
[23] Nelson MR, Thulin E, Fagan PA, et al. The ef-hand domain: a globally cooperative structural unit. Protein Sci 2002;11:198–205.
[24] Fransson A, Ruusala A, Aspenstom P. The atypical rho gtpases miro-1 and miro-2 have essential roles in mitochondrial trafficking. Biochem Biophys Res Commun 2006;344:500–10.
[25] MacAskill AF, Rinholm JE, Twelvetrees AE, et al. Miro1 is a calcium sensor for glutamate receptor-dependent localization of mitochondria at synapses. Neuron 2009;61:541–55.
[26] Saotome M, Safiulina D, Szabadkai G, et al. Bidirectional Ca^{2+}-dependent control of mitochondrial dynamics by the miro gtpase. Proc Natl Acad Sci USA 2008;105:20728–33.
[27] Liu X, Hajnoczky G. Ca^{2+}-dependent regulation of mitochondrial dynamics by the miro-milton complex. Int J Biochem Cell Biol 2009;41:1972–6.
[28] Liu S, Sawada T, Lee S, et al. Parkinson's disease-associated kinase pink1 regulates miro protein level and axonal transport of mitochondria. PLoS Genet 2012;8:e1002537.
[29] Wang X, Winter D, Ashrafi G, et al. Pink1 and parkin target miro for phosphorylation and degradation to arrest mitochondrial motility. Cell 2011;147:893–906.
[30] Boussif O, Lezoualc'h F, Zanta MA, et al. A versatile vector for gene and oligonucleotide transfer into cells in culture and in vivo: polyethylenimine. Proc Natl Acad Sci USA 1995;92:7297–301.
[31] Sun N, Malide D, Liu J, et al. A fluorescence-based imaging method to measure in vitro and in vivo mitophagy using mt-keima. Nat Protoc 2017;12:1576–87.
[32] Koury ST, Koury MJ, Bondurant MC. Cytoskeletal distribution and function during the maturation and enucleation of mammalian erythroblasts. J Cell Biol 1989;109:3005–13.
[33] Karbowski M, Neutzner A, Youle RJ. The mitochondrial e3 ubiquitin ligase march5 is required for drp1 dependent mitochondrial division. J Cell Biol 2007;178:71–84.
[34] Neuspiel M, Schauss AC, Braschi E, et al. Cargo-selected transport from the mitochondria to peroxisomes is mediated by vesicular carriers. Curr Biol 2008;18:102–8.
[35] Klosowiak JL, Park S, Smith KP, et al. Structural insights into parkin substrate lysine targeting from minimal miro substrates. Sci Rep 2016;6:33019.
[36] Klosowiak JL, Focia PJ, Chakravarthy S, et al. Structural coupling of the ef hand and c-terminal gtpase domains in the mitochondrial protein miro. EMBO Rep 2013;14:968–74.
[37] Luongo TS, Lambert JP, Gross P, et al. The mitochondrial Na^+/Ca^{2+} exchanger is essential for Ca^{2+} homeostasis and viability. Nature 2017;545:93–7.
[38] Mallilankaraman K, Doonan P, Cardenas C, et al. Micu1 is an essential gatekeeper for mcu-mediated mitochondrial Ca^{2+} uptake that regulates cell survival. Cell 2012;151:630–44.
[39] Hajnoczky G, Csordas G, Das S, et al. Mitochondrial calcium signalling and cell death: approaches for assessing the role of mitochondrial Ca^{2+} uptake in apoptosis. Cell Calcium 2006;40:553–60.
[40] Hajnoczky G, Hager R, Thomas AP. Mitochondria suppress local feedback activation of inositol 1,4, 5-trisphosphate receptors by Ca^{2+}. J Biol Chem 1999;274:14157–62.
[41] Paillard M, Csordas G, Huang KT, et al. Micu1 interacts with the d-ring of the mcu pore to control its Ca^{2+} flux and sensitivity to ru360. Mol Cell 2018;72:778–85.
[42] Bernardi P, Petronilli V. The permeability transition pore as a mitochondrial calcium release channel: a critical appraisal. J Bioenerg Biomembr 1996;28:131–8.
[43] De Stefani D, Rizzuto R, Pozzan T. Enjoy the trip: calcium in mitochondria back and forth. Annu Rev Biochem 2016;85:161–92.
[44] Elrod JW, Wong R, Mishra S, et al. Cyclophilin d controls mitochondrial pore-dependent Ca^{2+}exchange, metabolic flexibility, and propensity for heart failure in mice. J Clin Invest 2010;120:3680–7.
[45] Hurst S, Hoek J, Sheu SS. Mitochondrial Ca^{2+} and regulation of the permeability transition pore. J Bioenerg Biomembr 2017;49:27–47.
[46] Lu X, Kwong JQ, Molkentin JD, et al. Individual cardiac mitochondria undergo rare transient permeability transition pore openings. Circ Res 2016;118:834–41.
[47] Palty R, Silverman WF, Hershfinkel M, et al. Nclx is an essential component of mitochondrial Na^+/Ca^{2+} exchange. Proc Natl Acad Sci USA 2010;107:436–41.
[48] Rasola A, Bernardi P. Mitochondrial permeability transition in Ca^{2+}-dependent apoptosis and necrosis. Cell Calcium 2011;50:222–33.
[49] Rasola A, Bernardi P. The mitochondrial permeability transition pore and its adaptive responses in tumor cells. Cell Calcium 2014;56:437–45.
[50] Grice S. Mitochondrial disease with abnormal mitochondrial morphology. Thesis for the masters degree. Department of Biochemistry, University of Oxford; 2010.
[51] Lopez-Domenech G, Higgs NF, Vaccaro V, et al. Loss of dendritic complexity precedes neurodegeneration in a mouse model with disrupted mitochondrial distribution in mature dendrites. Cell Rep 2016;17:317–27.
[52] Nguyen TT, Oh SS, Weaver D, et al. Loss of miro1-directed mitochondrial movement results in a novel murine model for neuron disease. Proc Natl Acad Sci USA 2014;111:E3631–40.
[53] Kundu M, Lindsten T, Yang CY, et al. Ulk1 plays a critical role in the autophagic clearance of mitochondria and ribosomes during reticulocyte maturation. Blood 2008;112:1493–502.
[54] Sandoval H, Thiagarajan P, Dasgupta SK, et al. Essential role for nix in autophagic maturation of erythroid cells. Nature 2008;454:232–5.

[55] Schweers RL, Zhang J, Randall MS, et al. Nix is required for programmed mitochondrial clearance during reticulocyte maturation. Proc Natl Acad Sci USA 2007;104:19500–5.
[56] Brickley K, Smith MJ, Beck M, et al. Grif-1 and oip106, members of a novel gene family of coiled-coil domain proteins: association in vivo and in vitro with kinesin. J Biol Chem 2005;280:14723–32.
[57] Glater EE, Megeath LJ, Stowers RS, et al. Axonal transport of mitochondria requires milton to recruit kinesin heavy chain and is light chain independent. J Biol Chem 2006;173:545–57.
[58] Ahmad T, Mukherjee S, Pattnaik B, et al. Miro1 regulates intercellular mitochondrial transport & enhances mesenchymal stem cell rescue efficacy. EMBO J 2014;33:994–1010.
[59] Weihofen A, Thomas KJ, Ostaszewski BL, et al. Pink1 forms a multiprotein complex with miro and milton, linking pink1 function to mitochondrial trafficking. Biochemistry 2009;48:2045–52.
[60] Shlevkov E, Kramer T, Schapansky J, et al. Miro phosphorylation sites regulate parkin recruitment and mitochondrial motility. Proc Natl Acad Sci USA 2016;113:E6097–106.
[61] Safiulina D, Kuum M, Choubey V, et al. Miro proteins prime mitochondria for parkin translocation and mitophagy. EMBO J 2019;38:e99384.
[62] Gomez-Sanchez R, Gegg ME, Bravo-San Pedro JM, et al. Mitochondrial impairment increases fl-pink1 levels by calcium-dependent gene expression. Neurobiol Dis 2014;62:426–40.
[63] Sun Y, Vashisht AA, Tchieu J, et al. Voltage-dependent anion channels (vdacs) recruit parkin to defective mitochondria to promote mitochondrial autophagy. J Biol Chem 2012;287:40652–60.
[64] Narendra D, Kane LA, Hauser DN, et al. P62/sqstm1 is required for parkin-induced mitochondrial clustering but not mitophagy; vdac1 is dispensable for both. Autophagy 2010;6:1090–106.
[65] Zesiewicz TA, Strom JA, Borenstein AR, et al. Heart failure in parkinson's disease: analysis of the united states medicare current beneficiary survey. Parkinsonism Relat Disord 2004;10:417–20.
[66] Piqueras-Floresa J, Lopez-Garcia A, Moreno-Reig A, et al. Structural and functional alterations of the heart in parkinson's disease. Neurol Res 2018;40:53–61.
[67] Billia F, Hauck L, Konecny F, et al. Pten-inducible kinase 1 (pink1)/park6 is indispensable for normal heart function. Proc Natl Acad Sci USA 2011;108:9572–7.
[68] Kubli DA, Zhang X, Lee Y, et al. Parkin protein deficiency exacerbates cardiac injury and reduces survival following myocardial infarction. J Biol Chem 2013;288:915–26.
[69] Kubli DA, Quinsay MN, Gustafsson AB. Parkin deficiency results in accumulation of abnormal mitochondria in aging myocytes. Commun Integr Biol 2013;6:e24511.
[70] Bender A, Krishnan KJ, Morris CM, et al. High levels of mitochondrial DNA deletions in substantia nigra neurons in aging and parkinson disease. Nat Genet 2006;38:515–7.
[71] Kraytsberg Y, Kudryavtseva E, McKee AC, et al. Mitochondrial DNA deletions are abundant and cause functional impairment in aged human substantia nigra neurons. Nat Genet 2006;38:518–20.
[72] Mizuno Y, Ohta S, Tanaka M, et al. Deficiencies in complex i subunits of the respiratory chain in parkinson's disease. Biochem Biophys Res Commun 1989;163:1450–5.
[73] Nakagawa-Hattori Y, Yoshino H, Kondo T, et al. Is parkinson's disease a mitochondrial disorder? J Neurol Sci 1992;107:29–33.
[74] Bowen BC, Block RE, Sanchez-Ramos J, et al. Proton mr spectroscopy of the brain in 14 patients with parkinson disease. AJNR Am J Neuroradiol 1995;16:61–8.
[75] Vincent A, Briggs L, Chatwin GFJ, et al. Parkin-induced defects in neurophysiology and locomotion are generated by metabolic dysfunction and not oxidative stress. Hum Mol Genet 2012;21:1760–9.
[76] Kang R, Zeng L, Xie Y, et al. A novel pink1- and park2-dependent protective neuroimmune pathway in lethal sepsis. Autophagy 2016;12:2374–85.

Jiu-Qiang Wang received his Ph.D. degree from the University of Chinese Academy of Sciences in 2013. He is currently working with Dr. Tie-Shan Tang at the State Key Laboratory of Membrane Biology, Institute of Zoology, Chinese Academy of Sciences. His research interest is mainly focused on the molecular mechanism of neurodegenerative diseases.

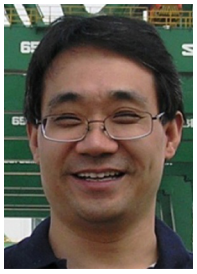

Tie-Shan Tang is a Professor of the State Key Laboratory of Membrane Biology, Chinese Academy of Sciences. Ongoing research activities in Dr. Tang's lab include: (1) discovering novel players that govern intracellular calcium homeostasis and crosstalk among organelles; (2) ER-mitochondrial calcium signaling axis in health and disease; (3) dysregulation of calcium signaling, DNA damage response and epigenomics in neural stem cell self-renewal and depletion; and (4) designing new/better treatment and prevention strategies for neurodegenerative diseases and tumors.